Atmospheric Aerosol Monitoring from Satellite Observations: A History of Three Decades

Kwon H. Lee, Zhanqing Li, Young J. Kim and Alexander Kokhanovsky

Abstract More than three decades have passed since the launch of the first satellite instrument used for atmospheric aerosol detection. Since then, various powerful satellite remote sensing technologies have been developed for monitoring atmospheric aerosols. The application of these new technologies to different satellite data have led to the generation of multiple aerosol products, such as aerosol spatial distribution, temporal variation, fraction of fine and coarse modes, vertical distribution, light absorption, and some spectral characteristics. These can be used to infer sources of major aerosol emissions, the transportation of aerosols, interactions between aerosols and energy and water cycles, and the involvement of aerosols with the dynamic system. The synergetic use of data from different satellite sensors provides more comprehensive information to better quantify the direct and indirect effects of aerosols on the Earth's climate. This paper reviews how satellite remote sensing has been used in aerosol monitoring from its earliest beginnings and highlights future satellite missions.

Keywords Satellite · Instrument · Remote sensing · Aerosol · Monitoring

1 Introduction

Atmospheric aerosols are defined as suspended particles (solid or liquid) in a gas medium. The particles that compose aerosols range in size from nanometers to tens of micrometers, depending on whether they originate from natural sources (e.g., pollens, sea-salt, wind-blown dust, volcanic ash) or from man-made sources (e.g., smoke, soot, biomass burning). Aerosols can contribute to a reduction in visibility (Trijonis et al. 1991) and a decline in human health (Davidson et al. 2005) as well as affecting climate change (IPCC 2007). To fully understand aerosol effects, their characteristics (quantity, composition, size distribution, and optical properties) must be known on local to global scales (Kaufman et al. 2002).

Aerosol properties have been typically acquired using ground-based point measurements. Details concerning aerosol properties have been obtained from in-situ measurements, such as from aircraft or balloons, but these were limited to a few aerosol intensive measurement campaigns. Examples of such campaigns include the International Global Atmospheric Chemistry (IGAC) programs (IGAC 1996), the Tropospheric Aerosol Radiation Forcing Observation Experiment (TARFOX) (Russell et al. 1999) and three Aerosol Characterization Experiments such as ACE-1 (Bates et al. 1998), ACE-2 (Raes et al. 2000), and ACE-Asia (Huebert et al. 2003). The use of satellites to monitor aerosols has the advantage of providing routine measurements on a global scale and is an important tool for use in improving our understanding of aerosol properties.

The first visual observations of atmospheric aerosol effects were made from the manned spacecrafts. Cosmonaut Yuri Gagarin observed clouds and their shadows, as well as optical phenomena due to the presence of aerosols, during the first manned space flight on the spacecraft Vostok on April 12, 1961. These first observations were visual in nature but in

K.H. Lee (✉)
Department of Atmospheric and Ocean Science, Earth System Science Interdisciplinary Center, University of Maryland, College Park, MD 20740, USA
e-mail: Kwonlee@umd.edu

Y.J. Kim et al. (eds.), *Atmospheric and Biological Environmental Monitoring*,
DOI 10.1007/978-1-4020-9674-7_2,

subsequent space flights, photography was used by cosmonaut G. S. Titov (Vostok-2, August 6, 1961), cosmonaut V. V. Tereshkova (Vostok-6, June 16, 1963), K. P. Feoktistov (Voskhod, October 12, 1964), A. A. Leonov (Voskhod-2, March 18, 1965), and others. They took photos of the horizon in order to estimate the vertical distribution of aerosols. A. G. Nikolaev and V. I. Sevastyanov (Soyuz-9, June 1, 1970) used hand-held spectrophotometers to measure the spectrometry of the twilight and daylight horizons, as well as that of clouds and snow. This instrument was also used in several follow-up missions. Stratospheric aerosol measurements using a hand-held sun photometer were made on the Apollo-Soyuz in 1975 (Pepin and McCormick 1976). Further information on the first instrumental observations of the planet from manned aircrafts is given by Lazarev et al. (1987).

The first detection of aerosols from an un-manned spacecraft was achieved by the Multi Spectral Scanner (MSS) onboard the Earth Resources Technology Satellite (ERTS-1) (Griggs 1975; Fraser 1976; Mekler et al. 1977) and the first operational aerosol products were generated from the TIROS-N satellite launched on 19 October 1978. The Advanced Very High Resolution Radiometer (AVHRR) onboard TIROS-N was originally intended for weather observations but its capability was expanded to the detection of aerosols. The Nimbus-7 was launched on 25 October 1978, carrying the Stratospheric Aerosol Measurement instrument (SAM) (McCormick et al. 1979) and the Total Ozone Mapping Spectrometer (TOMS). While the TOMS was not originally designed for aerosol monitoring, it has since provided the longest measurement record of global aerosols from space (Herman et al. 1997; Torres et al. 2002). These launches thus marked the beginning of an era of satellite-based remote sensing of aerosols that has lasted over three decades to date.

Advances in satellite monitoring capabilities have resulted in the generation of many valuable scientific datasets from local to global scales, which are useful to researchers, policy makers, and the general public. Satellite instruments give us the ability to make more accurate measurements on a nearly daily basis across a broader geographic area and across a longer time frame. This paper reviews various space-borne sensors used in the remote sensing of aerosols and the associated data products retrieved from satellite measurements. Section 2 presents an overview of satellite remote sensing data and instruments. Various aerosol retrieval techniques applied to satellite data is introduced in Section 3. In Section 4, the acquisition of satellite data and applications, including inter-comparisons, climatologies, and synergy studies, are discussed. The prospects for future missions are highlighted as well.

2 Satellite Observations for Aerosol Monitoring

Space agencies, such as the National Aeronautics and Space Administration (NASA), the National Ocean and Atmosphere Administration (NOAA), the European Space Agency (ESA), le Centre National d'Etudes Spatiales (CNES) in France, the Japanese Aerospace Exploration Agency (JAXA), the China Meteorological Administration, the Royal Netherlands Meteorological Institute (KNMI), and the German Aerospace Centre (DLR), have launched many satellite instruments. Table 1 shows a timeline of satellite missions from 1972 to 2006 and a summary of the features for each sensor. Aerosol monitoring from space has, in the past, been accomplished using satellite data not explicitly designed with this application in mind. Historical satellite observations still in operation are the TOMS and AVHRR series. The AVHRR has been primarily used for the surveillance of weather systems and the monitoring of sea surface temperatures (SST) and land vegetation indices (VI). The TOMS was originally designed for deriving the total ozone content in the atmosphere. As a by-product, aerosol information has been successfully extracted from both sensors, such as aerosol optical depth/thickness (AOD/AOT, τ) from the AVHRR (Stowe et al. 1997) and the UV-absorbing aerosol index (AI) from the TOMS (Herman et al. 1997; Hsu et al. 1999).

Information concerning aerosols was also inferred from other later sensors, such as the Sea-viewing Wide Field-of-view Sensor (SeaWiFS), and the Moderate Resolution Imaging Spectro-radiometer (MODIS); the near-future Visual/Infrared Imager Radiometer Suite (VIIRS) will continue in this vein. The SeaWiFS, developed for studying marine biogeochemical processes, has been employed to produce aerosol

Table 1 The history of platforms and sensors used to derive aerosol properties from space

Launch	End	Platform	Instrument	# of bands (wavelengths (μm))	Accuracy	Reference[a]
1972	1978	Landsat(ERTS-1)	MSS	4(0.5–1.1)	τ(10%)	Griggs (1975)
1974	1981	SMS-1, 2	VISSR	5(0.65–12.5)		
1975	Present	GOES-1∼12	VISSR	5(0.65–12.5)	τ(18∼34%)[b]	Knapp et al. (2002)
1975	1975	Apollo-Soyuz	SAM	0.83	–	McCormick et al. (1979)
1977	2005	GMS-1∼5	VISSR	4(0.45–12.5)	–	–
1978	1980	TIROS-N	AVHRR	4(0.58–11.5)	–	–
1978	1993	Nimbus-7	SAM-2,	1	σ_{ext}(10%)	McCormick et al. (1979)
			CZCS,	6(0.443–11.5)	–	–
			TOMS	6(0.312–0.380)	–	–
1979	1981	AEM-B	SAGE	4(0.385,0.45,0.6,1.0)	σ_{ext}(10%)	Chu and McCormick (1979)
1979	Present	NOAA-6∼16	AVHRR	5(0.58–12)	τ(10%)[c], τ(3.6%)[d]	Stowe et al. (1997)
						Mishchenko et al. (1999)
1984	2005	ERBS	SAGE-2	4(0.386–1.02)	σ_{ext}(10%)	Chu et al. (1989)
1997	Present	TRMM	VIRS	5(0.63–12)	τ(35%), α(±0.5)	Ignatov and Stowe (2000)
1991	1996	SPOT-3	POAM-2	9(0.353–1.060)	σ_{ext} (∼20%)	Randall et al. (1996)
1991	1999	ERS-1	ATSR,	4(1.6, 3.7, 11, 12)	–	–
			GOME	4(0.24–0.79)	–	Torricella et al. (1999)
1992	2005	UARS-	HALOE	8(2.45–10.01)	r_{eff}(±15%), σ_{ext}(±5%)	Hervig et al. (1998)
1994	1994	SSD	LITE	3(0.355, 0.532, 1.064)	$\beta(\lambda_1)/\beta(\lambda_2)$(<5%)	Gu et al. (1997)
1995	Present	ERS-2	ATSR-2,	7(0.55–12)	τ(<0.03), τ(30%)	Veefkind et al. (1999)
			GOME	0.24–0.79		
1996	Present	Earth Probe	TOMS	6(0.309–0.360)	τ(20∼30%)[e]	Torres et al. (2002)
1996	1997	ADEOS	POLDER,	9(0.443–0.910)	τ(20∼30%)[f],	Herman et al. (1997)
			ILAS,	2(0.75–0.78, 6.21–11.77)	–	–
			OCTS	7(0.412–0.865)	–	–
1997	Present	OrbView-2	SeaWiFS	8(0.412–0.865)	T(5∼10%)	Gordon and Wang (1994)
1998	Present	SPOT-4	POAM-3	9(0.354–1.018)	σ_{ext}(±30%)	Randall et al. (2001)
1999	Present	TERRA	MODIS,	36 (0.4–14.4)	τ(5∼15%)[g],	Remer et al. (2005)
			MISR	4 (0.45∼0.87)	τ(10∼20%)	Kahn et al. (2005)
2001	2005	METEOR-3M	SAGE-3	9(0.385–1.545)	σ_{ext}(5%), τ(5%)	Thomason et al. (2007)
2001	Present	PROBA	CHRIS	62(0.4–1.05)	–	Barnsley et al. (2004)
2001	Present	Odin	OSIRIS	0.274–0.810	σ_{ext}(15%)	Bourassa et al. (2007)
2002	Present	AQUA	MODIS	–	–	–
2002	Present	ENVISAT	AATSR,	7(0.55∼12.0)	τ(0.16),	Grey et al. (2006)
			MERIS,	15(0.4–1.05)	τ(∼0.2),	Vidot et al. (2008)
			SCIAMACHY	0.24–2.4	AI(∼0.4)	Graaf and Stammes (2005)
2002	2003	ADEOS-2	POLDER-2,	9(0.443–0.910)	–	–
			ILAS-2,	4(0.75–12.85)	–,	Zasetsky and Sloan (2005)
			GLI	36(0.38–12)	τ(∼0.1)	Murakami et al. (2006)
2002	Present	MSG-1	SEVIRI	12(0.6–13.4)	τ(0.08)	Popp et al. (2007)
2003	2003-	ICEsat	GLAS	2(0.532, 1.064)	σ_{ext}(10%),τ(20%)	Palm et al. (2002)
2004	Present	AURA	OMI,	3(0.27–0.5)	τ(30%),	Torres et al. (2007),
			HIRDLS	21(6–18)	σ_{ext}(5∼25%)	Froidevaux and Douglass (2001)
2004	Present	PARASOL	POLER-3	8(0.44–0.91)	–	–
2006	Present	CALIPSO	CALIOP	2(0.532, 1.064)	–	–

[a]References of the validation study for accuracy listed here.
[b]Accuracy for operational GOES aerosol retrieval may apply for other GOES series.
[c]Accuracy for single channel AVHRR aerosol retrieval algorithm may apply for other AVHRR series.
[d]Accuracy for two channel AVHRR aerosol retrieval algorithm may apply for other AVHRR series.
[e]Accuracy for TOMS AOT retrieval from Nimbus-7 to Earth Probe.
[f]may apply for the POLDER-2 and -3.
[g]same to the MODIS/Aqua.

data required for atmospheric correction (Gordon and Wang 1994). With the launch of Terra (EOS AM-1), more advanced instruments like MODIS and the Multiangle Imaging SpectroRadiometer (MISR) provide substantially improved aerosol retrievals (Remer et al. 2005; Diner et al. 1998). The same applies to the Medium Resolution Imaging Spectrometer (MERIS) and Advanced Along-Track Scanning Radiometer (AATSR) onboard the ESA EnviSAT. The launch of POLDER on ADEOS II added more capabilities by virtue of its polarization measurements of backscattered solar light (Leroy et al. 1997). Space-borne light detection and ranging (LIDAR) observations from the Lidar In-space Technology Experiment (LITE) (Winker et al. 1996), the Geoscience Laser Altimeter System (GLAS) (Spinhirne et al. 2005a, b), and the most recently launched Cloud-Aerosol Lidar and Infrared Pathfinder Satellite Observations (CALIPSO) (Vaughan et al. 2004) allow for global-scale assessments of the vertical distribution of aerosols, backscatter, extinction, and depolarization ratios.

In terms of information content, satellite data may be classified into three general categories. The first is aimed at portraying the spatial and temporal dynamics of aerosol loading. The second is concerned with columnar aerosol properties retrievals (e.g., aerosol columnar mass retrievals) through use of spectral, polarization, and angular characteristics of backscattered solar light. The third provides information on the vertical profile of aerosols from the surface into the stratosphere. Contingent upon the need of a particular aerosol attribute, a single sensor or combination of sensors may be used.

There are two basic types of satellite instruments depending on the observation geometry, namely vertical and horizontal measurements (Fig. 1). By vertical (or nadir viewing) observation, the instrument faces to nadir or near-nadir and senses the radiation coming from the Earth. Most instruments employ this concept to provide column integrated products. Observation in horizontal direction including Limb-viewing and occultation sounding, probes the Earth's limb at various depths in the atmosphere. This observation is characterized by the altitude and the geolocation of the tangent point. Especially, solar occultation instruments can retrieve aerosol extinction profile from measurement of sunlight extinction through the atmospheric limb during sunrise and sunset. All these methods require accurate calibration of instruments and sound

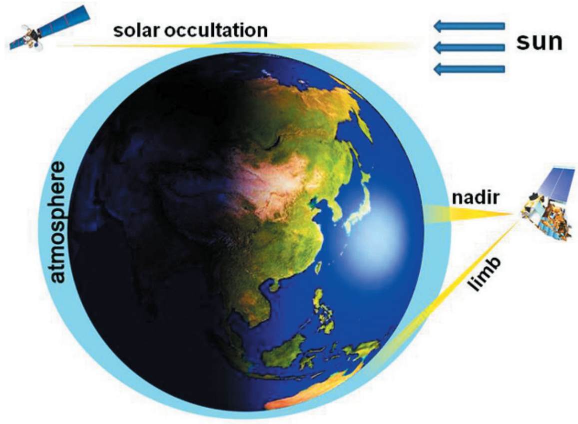

Fig. 1 Vertical (nadir) and horizontal (limb and solar occultation) satellite observation concept. Nadir viewing is looking straight down to measure columnar observation. Limb viewing provides a much longer path through the atmosphere, and also makes it easier to determine the altitudes of the observed substances

treatment of unknown optical properties of aerosols, surface reflectivity, and gaseous absorption.

Inference of aerosol properties from satellite relies on the interaction of electromagnetic radiation scattered and/or absorbed by the atmospheric constituents and the surface target as illustrated in Fig. 2. Radiation is received by two basic types of sensors: passive and active. Passive sensors record radiation emitted by the Sun and reflected back to the sensor while active sensors receive energy emitted by the sensor itself (laser beam). Aerosol remote sensing is an ill-posed problem because the number of variables to be determined is larger than the number of parameters, which can be in principle found and constrained from the satellite measurements themselves. The essence of aerosol remote sensing is to decompose mixed signals emanating from atmospheric gases, aerosols, and the surface, after clouds are filtered out. Reflectance, the ratio of radiances received by a sensor over that reaching the top of atmosphere (TOA) in a particular direction, can be expressed by the following equation:

$$\rho_{TOA}(\theta_0, \theta_S, \phi) = \rho_{atm}(\theta_0, \theta_S, \phi) + \frac{T_0(\theta_0) \cdot T_S(\theta_S) \cdot A_g}{1 - s \cdot A_g} \quad (1)$$

where $\rho_{atm}(\theta_0, \theta_S, \phi)$ is the reflectance by the atmosphere, and $T_0(\theta_0)$ and $T_S(\theta_S)$ are downward and

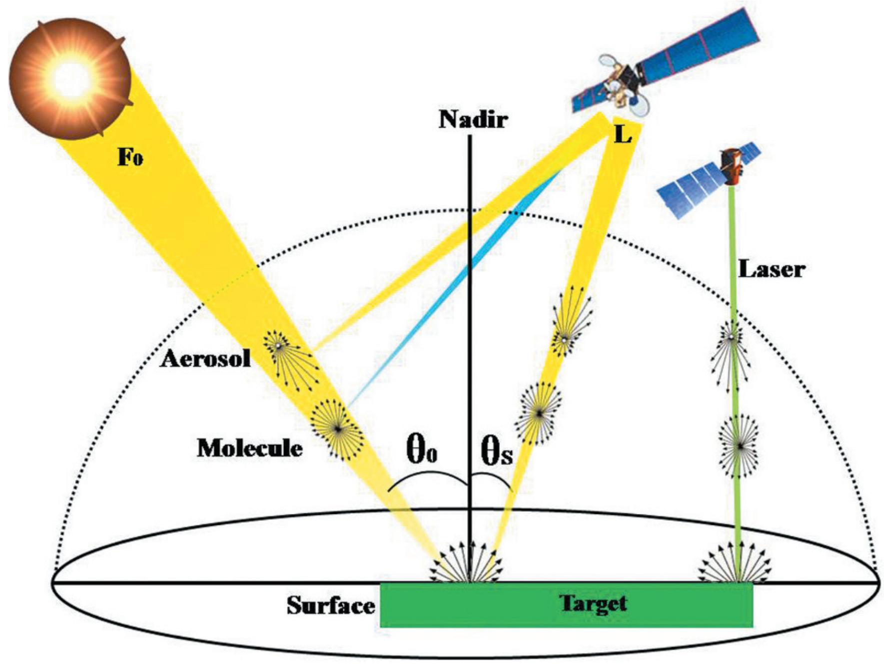

Fig. 2 Basic scheme of radiative transfer processes for passive and active satellite remote sensing

upward total transmission (diffuse plus direct); θ_S is the satellite zenith angle, θ_0 is the solar viewing angle, and ϕ is the relative azimuth angle. The spherical albedo is given by s and A_g is the surface reflectance. It follows from Eq. (1) that the signal received by a satellite sensor is dictated by atmospheric variables (gases, aerosols, cloud hydrometeors, etc.) and surface variables. When a cloud is present, reflection by the cloud is often overwhelming. As such, the first step is to identify the presence of clouds. Aerosol remote sensing is only valid under clear-sky conditions. Any cloud contamination can easily confuse the faint signal of aerosols, whereas excessive cloud screening may remove pixels containing heavy aerosol loading. Due to the delicacy of cloud screening, it remains the largest uncertainty in aerosol retrievals (Jeong and Li 2005). The second step is to account for molecular scattering due to atmospheric molecules and gas absorption. The Rayleigh path radiance can be determined using the spectral dependence of the well-known Rayleigh optical depth (ROD) and the Rayleigh phase function. The third step is to remove surface reflection from satellite-received signal. Early attempts at aerosol retrievals (Griggs 1975; Mekler et al. 1977; Durkee et al. 1986; Stowe 1991; Higurashi and Nakajima 1999; Mishchenko et al. 1999; Deuzé et al. 1999) were limited to dark surfaces with low and uniform reflectivities, such as oceans. However, aerosol remote sensing over brighter land surfaces is very important for environmental and climate studies because most aerosols originate from continental sources such as bare soil, deserts, urban, industrial, and agricultural areas. Aerosol retrieval over land requires accurate knowledge of surface reflectance, and its spectral and angular dependence. The first attempt of aerosol retrieval over land is found in Kaufman and Joseph (1982). Thanks to the advent of new remote sensing techniques developed by taking advantage of multi-angle and multi-spectral measurements (Kaufman et al. 1997; Martonchik et al. 1998, 2002; Hsu et al. 2004; Remer et al. 2005; Levy et al. 2007b), such a limitation has been eliminated or lessened considerably.

3 Satellite Aerosol Remote Sensing Techniques

Many algorithms have been developed for aerosol detection using satellite measurements made at single- or multiple-wavelengths, nadir view and multi-angle views, with or without polarization, and low earth or geostationary orbits. Some of the algorithms are used for routine applications, while others are used for research and development. Numerous attempts were also made to compare and assess different satellite aerosol products, including those from the MODIS, MISR, AVHRR, TOMS, SeaWiFS, MERIS, AATSR, and other instruments (Myhre et al. 2004; Jeong et al. 2005; Jeong and Li 2005; Kokhanovsky et al. 2007; Kokhanovsky and de Leeuw 2009). The accuracies of various aerosol retrievals are summarized in Table 1. It must be remarked, however, that the estimations of the errors of the aerosol retrieval algorithms are given usually after analyzing large statistical ensembles of coincident ground and satellite spectral AOT measurements. Therefore, errors for any given measurement can be much larger as compared to the average error for the ensemble. The principles and limitations of these algorithms for tropospheric aerosols were previously reviewed by King et al. (1999). This paper reviews a number of aerosol retrieval techniques and categorizes them according to location in the atmosphere (troposphere and stratosphere) and from single- and multi-sensor data. An overview of the different techniques is outlined below.

3.1 Geostationary Satellite Algorithm

Although the AOT inferred from polar (or low orbit) satellite measurements provide global coverage map with fine spatial resolution, these observations are limited in space and time. The geostationary satellite measurements provide a unique tool for quantifying aerosol properties with high temporal resolution. Aerosol retrieval from geostationary observations has advantage in the obtaining of surface reflectance information from 'background image' acquired from composited minimum reflectance values among numerous views of the same location for a period. The AOT can be then retrieved by comparing imagery to this 'background image' (Knapp and Stowe 2002; Knapp et al. 2005). The uncertainty of the operational GOES AOT retrieval was reported as ±18–34% (Knapp and Stowe 2002; Knapp et al. 2002). Other geostationary satellites such as METEOSAT and GMS have been frequently used to derive aerosol properties (Dulac et al. 1992; Moulin et al. 1997; Wang et al. 2003; Costa et al. 2006).

3.2 Single-Channel AVHRR Algorithm

The most used single channel for aerosol retrievals is channel 1 of the AVHRR (the wavelength $\lambda = 0.63\,\mu$m) (Rao et al. 1989; Stowe 1991; Stowe et al. 1997; Ignatov et al. 1995a). The AVHRR algorithms are generally developed based on the look-up table (LUT) calculated using radiative transfer codes such as Dave (1973) and by assuming certain types of aerosol models. In an earlier algorithm (Stowe 1991), non-absorbing ($n = 1.5$–$0.0i$) aerosols with a size distribution following a modified Junge size distribution were assumed.

$$\begin{aligned}\frac{dN}{dr} &= 0 \quad (\mathrm{r} < \mathrm{r_{min}}, \mathrm{r} > \mathrm{r_{max}}) \\ &= A(\mathrm{r_{min}} \le \mathrm{r} \le \mathrm{r_m}) \\ &= A\left(\frac{r}{r_m}\right)^{-(\upsilon+1)} (\mathrm{r_m} \le \mathrm{r} \le \mathrm{r_{max}}) \end{aligned} \tag{2}$$

where, r_{min}, r_{m}, r_{max} are particle radii equal to 0.03, 0.1, and 10 μm, respectively; size parameter $\upsilon = 3.5$, the normalized constant A. The retrieval results were validated against ship-borne sun-photometer measurements made within ±2 hours of the satellite overpass (Ignatov et al. 1995b). The comparison shows a negative bias, i.e. $\tau_{\mathrm{sat}} = 0.64 \cdot \tau_{\mathrm{sp}} - 0.02$ (Stowe 1997).

The algorithm currently used for generating operational AVHRR aerosol products, known as AVHRR Pathfinder Atmosphere (PATMOS) (Stowe et al. 2002; Jacobowitz et al. 2003) uses a lognormal aerosol size distribution

$$\frac{dN}{dr} = \frac{A}{\sqrt{2\pi}\, r \ln\sigma} \exp\left[-\frac{1}{2}\cdot\left(\frac{\ln r - \ln r_m}{\ln\sigma}\right)^2\right] \tag{3}$$

where $r_m = 0.1\,\mu$m, $\sigma = 2.03$ with a refractive index $n = 1.4$–$0.0i$, and the Fresnel model to account for the bidirectional reflectance of a calm ocean surface (Viollier et al. 1980; Gordon and Morel 1983). These adjustments bring satellite AOT retrievals into agreement with surface observations to better than 10%. The liner regression between the two is $\tau_{\mathrm{sat}} = 0.91\tau_{\mathrm{sp}} + 0.01$ (Stowe et al. 1997).

3.3 Dual-Channel AVHRR Algorithm

The Ångström exponent (α), a parameter used to denote aerosol particle size, can be derived using both AVHRR shortwave channels ($\lambda = 0.65$, $0.85\,\mu$m) (Stowe et al. 1997; Mishchenko et al. 1999; Geogdzhayev et al. 2002). The two-channel algorithm has been applied to the International Satellite Cloud Climatology Project (ISCCP) cloud-free product (Rossow et al. 1996) to generate the Global Aerosol Climatology Product (GACP). Aerosols are assumed to be spherical with the power-law size distribution and a refractive index of 1.5–0.003i. In principle, two-channel algorithms are expected to provide more accurate retrievals than one-channel algorithms. However, because there is no onboard calibration of the instrument, the accuracy of the algorithms is more susceptible to calibration errors in both channels. Both single-channel and dual-channel algorithms are most sensitive to cloud screening errors, which is by far the largest source of errors in retrieving aerosol parameters.

It is worth noting that the retrieval of AOT is very sensitive to the choice of aerosol size distribution and complex refractive indices. For the same TOA reflectance, use of two distinct distribution functions (power law and bi-modal log-normal distributions), as adopted by the GACP and MODIS algorithms, can account for a large portion of the discrepancies in AOT retrievals (Jeong et al. 2005). Geogdzhayev et al. (2002) and Knapp et al. (2002) also showed that the imaginary part of the refractive index can also affect AOT retrieval. Unfortunately, there is no consensus as to which size distribution is more representative on a global scale. Many factors can change the aerosol size distribution, such as aerosol type, humidity, season and location, etc.

3.4 TOMS Algorithm

The TOMS instrument has flown on Nimbus-7, ADEOS and EP-TOMS since 1978, providing the longest record of data for monitoring ozone depletion. Hsu et al. (1996) found that the ratio of its two channels (331 and 360 nm) is sensitive to absorbing aerosols and an aerosol index (AI) was defined as (Herman et al. 1997) and is given by:

$$AI = -100 \log_{10} \left[\left(\frac{I_{340}}{I_{380}} \right)_{meas} - \left(\frac{I_{340}}{I_{380}} \right)_{calc} \right] \quad (4)$$

where I_{meas} and I_{calc} are the measured and calculated backscattered radiances at the two wavelengths. Under the existence of absorbing aerosols, I_{meas} is smaller than I_{calc} predicted by the Dave's Lambert Equivalent Reflectivity (LER) model (McPeters et al. 1996) so produces positive residues, and vice-versa for non-absorbing aerosols. One of the unique strengths of this technique is that since clouds produce nearly zero residues, the presence of subpixel clouds does not affect the detection of aerosols (Herman et al. 1997). Daily global TOMS AI products have been generated and are widely employed to detect and monitor the spatial and temporal variations of elevated smoke and dust and other types of absorbing aerosols.

Attempts were also made to extract additional quantitative aerosol parameters, such as AOT and single scattering albedo (SSA) (Herman et al. 1997; Torres et al. 1998). Unlike the AI, which is mainly sensitive to UV-absorbing aerosols, the TOMS near-UV AOT retrieval algorithm is sensitive to all aerosol types. However, this retrieval is affected by the aerosol layer altitude, the single-scattering albedo, and subpixel cloud contamination due to its large footprint (about $40\,\text{km}^2$ at nadir) (Herman et al. 1997; Torres et al. 1998, 2002). Torres et al. (2002) presented the first long-term (1979 to present) nearly-global climatology of AOT over both land and ocean with a retrieval uncertainty of ∼30% relative to Aerosol Robotic Network (AERONET) observations, while the AOT of non-absorbing aerosols agreed to within 20%. The SSA derived from TOMS generally agrees within 0.03 of AERONET retrievals (Torres et al. 2005). The main constraint on the capability of the technique lies in the lack of information on aerosol type, vertical distribution and surface reflectance. The retrieval algorithm, called the 'near-UV algorithm', uses two backscattered radiances at near-UV bands. Three major aerosol types are assumed for the construction of the LUT and the examination of the variability of the relationship between the spectral contrast and the radiance at the longer wavelength. These LUTs are used to determine AOT and SSA.

3.5 Ocean Color Algorithms (CZCS, SeaWiFS, OCTS, MODIS)

The aerosol retrieval from ocean color sensors begins with the following equation (Gordon and Wang 1994):

$$\rho_{TOA}(\lambda) = \rho_r(\lambda) + \rho_a(\lambda) + \rho_{ra}(\lambda) + \rho_g(\lambda) + t \cdot \rho_w(\lambda) \tag{5}$$

where $\rho_r(\lambda)$, $\rho_a(\lambda)$, $\rho_{ra}(\lambda)$, $\rho_g(\lambda)$, and $\rho_w(\lambda)$ represent reflectances due to multiple scattering by air molecules (Rayleigh scattering), aerosols, the interaction between molecular and aerosol scattering which is negligible in the single-scattering case, the rough ocean surface which is also negligible because of low reflection over the ocean and the tilting sensor, and the water-leaving reflectance, respectively. The atmospheric transmission is represented by t. By using a set of aerosol models, aerosol effects at near-infrared (NIR) bands can be evaluated from Eq. (5) because $\rho_w(\lambda)$ at these bands are usually negligible for the open ocean waters due to strong water absorption (Hale and Querry 1973; Smith and Baker 1981).

Aerosol products are by-products from the atmospheric correction for the ocean color algorithm (Gordon and Wang 1994). Using Eq. (5), the $\rho_a(\lambda)$ values are derived from ocean color observations, then used to select the two most appropriate aerosol models from a set of LUTs. The current SeaWiFS and MODIS ocean color data processing algorithms use 12 aerosol models for generating the LUTs (Wang et al. 2005). They are the Oceanic model with 99% RH, the Maritime model and the Coastal model with an RH of 50, 70, 90, and 99%, and the Tropospheric model with an RH of 50, 90, and 99%, respectively. A weight that is best-fit to the measured NIR radiances from the radiances computed using the two selected aerosol models. Using the two aerosol models with the weight and the satellite measured radiance, the AOT and Ångström exponent can then be retrieved (Gordon and Wang 1994).

3.6 Polarization (POLDER, POLDER-2, POLDER-3)

The POLDER measures the polarization, directional, and spectral characteristics of solar light reflected by aerosols. A scientific goal of the POLDER experiment was to determine the physical and optical properties of aerosols so as to classify them and study their variability and cycles (Herman et al. 1997; Deuzé et al. 1999). The POLDER instrument is a push-broom-type, wide field-of-view, multi-band imaging radiometer and polarimeter with eight narrow spectral bands in the visible and near infrared (0.443, 0.490, 0.565, 0.665, 0.763, 0.765, 0.865, and 0.910 μm). The spectral variation allows the derivation of the aerosol size and thus their scattering phase function, as well as the AOT. The polarization provides some information on the aerosol refractive index and shape (spherical or non-spherical), which improves the determination of the scattering phase function. The algorithm is based on LUTs from POLDER directional, spectral and polarized measurements for several aerosol models. Using this unique information from POLDER measurements, Breon et al. (2002) found that the effect of aerosols on cloud microphysics is significant and occurs on a global scale. The accuracy in AOT retrieval was reported as 30% (Herman et al. 1997). The Ångström exponent derived from POLDER data correlated well with AERONET data, although it is also systematically underestimated by 30% (Goloub et al. 1999).

3.7 Multi-Channel Algorithm (SeaWiFS, MODIS, MERIS)

The MODIS instrument is deployed on both the Terra (EOS-AM) and Aqua (EOS-PM) satellites and measures upwelling radiances in 36 bands for wavelengths ranging from 0.4 to 14.5 μm. With a spatial resolution of 250, 500 m, or 1 km at nadir, MODIS data have been employed to generate the most comprehensive aerosol products including AOT, fine mode fraction (FMF), effective radius of aerosol particles (equal to the ratio of the third to the second moment of the aerosol size distribution), and mass concentration (Kaufman et al. 1997; Tanré et al. 1997, 1999; Remer et al. 2005). The retrieval uncertainty of the MODIS AOT products falls within the expected range of $\pm 0.03 \pm 0.05\tau_{sat}$ over ocean and $\pm 0.05 \pm 0.15\tau_{sat}$ over land (Remer et al. 2005; Chu et al. 2002). While the expected accuracy is met in general, significantly larger errors are found in certain regions (Levy et al. 2005; Li et al. 2007), especially where no or few ground measurements were available to train the algorithm. To remedy some of the problems, modifications were introduced by Levy et al. (2007a) to better account for the effects of surface spectral and bidirectional reflectance, as well as aerosol absorption. The modified algorithm is now used to generate the Collection 5 (C005) product (Remer et al. 2006). Over land, the C005 product has a significantly improved accuracy when compared to the earlier version of the product, as was shown in some validation studies using ground-based AERONET data (Levy et al. 2007b; Mi et al. 2007) and hand-held sunphotometer data in China (Li et al. 2007).

Retrieving aerosol properties from satellite remote sensing over a bright surface is a challenging problem. The Bremen Aerosol Retrieval (BAER) is capable of retrieving AOT over land surfaces and was first developed by von Hoyningen-Huene et al. (2003). It is based on the assumption that the surface reflectance is comprised of the mixed spectra from vegetation and bare soil. The fraction of vegetation in the pixel is estimated in an iterative way tuned by the NDVI. This method is very flexible to use for aerosol retrieval with visible satellite observation data. Applications of the BAER algorithm and validation has been reported for the SeaWiFS (von Hoyningen-Huene et al. 2003; Lee et al. 2004), MERIS (von Hoyningen-Huene et al. 2006), SCIAMACHY (von Hoyningen-Huene et al. 2005), and MODIS (Lee et al. 2005, 2006a, b, 2007a).

Hsu et al. (2004) proposed a new approach, called ‘Deep Blue’, to retrieve aerosol properties over bright land surfaces such as arid, semiarid, and urban areas. Those areas are typically very bright in the red to the NIR spectral region, but are relatively darker in the blue-band region. Using the global surface reflectance database of 0.1×0.1-degree resolution from the minimum reflectivity technique (e.g., finding the clearest scene during each season for a given location), the contribution of the surface-reflected radiance can be separated from the satellite-receiving radiance. Aerosol properties including AOT and aerosol type can then be determined simultaneously in the algorithm using LUTs. Comparisons of the satellite AOT and the AERONET AOT indicate good agreement (i.e., within 30%) over sites in Nigeria and Saudi Arabia (Hsu et al. 2004) and over East Asia (Hsu et al. 2006).

3.8 Multi-Angle, Multi-Channel (MISR)

The MISR instrument shares the Terra platform with the MODIS and uses nine individual CCD-based pushbroom cameras to view Earth at nine different view angles: one at nadir and eight symmetrical views at 26.1, 45.6, 60.0, and 70.5 degrees forward and aft of nadir. Each camera obtains images at four spectral bands (443, 558, 672, and 866 nm) with a horizontal resolution of 1.1 km in non-red bands and 275 m in the red band (Diner et al. 1998). To retrieve spectral AOT and additional properties such as the Ångström exponent, SSA, number fraction, and volume fraction, the MISR offers a unique combination of multiple bands and multi- angles that convey richer information about aerosols (Martonchik and Diner 1992; Martonchik et al. 1998, 2002; Diner et al. 2008). The retrieval algorithm differs over water, dense dark vegetation (DDV), and heterogeneous land (Martonchik et al. 1998, 2002). For dark water, zero water-leaving radiances at red and near-infrared wavelengths are considered, which is similar to the ocean color algorithm. The algorithm for DDV uses an angular shape for the surface bidirectional reflectance factor (BRF) with angular measurements. For heterogeneous land, empirical orthogonal functions derived from the spectral contrast by multi-angle observations are used to determine AOT and the aerosol model.

Validation of MISR AOTs using AERONET AOTs has been reported in many studies. The comparisons show a positive bias of 0.02 with an overestimation of 10% over southern Africa (Diner et al. 2001), an overestimation of about 0.05 over China (Christopher and Wang 2004), a linear relationship of $\tau_{sat} = 0.92\tau_{sp} + 0.02$ ($R^2 = 0.90$) and a retrieval error of $0.04 \pm 0.18\tau_{sp}$ over the United States (Liu et al. 2004), an uncertainty of 0.08 in desert areas (Martonchik et al. 2004), and linear relationships in the red and blue bands of $\tau_{sat} = 0.74\tau_{sp} + 0.11$ ($R = 0.87$) and $\tau_{sat} = 0.83\tau_{sp} + 0.03$ ($R = 0.86$), respectively, over various AERONET sites (Abdou et al. 2005). Kahn et al. (2005) reported that from a two-year comparison, about two-thirds of the MISR-retrieved AOT values fall within 0.05 or 20% of AERONET AOTs and more than a third are within 0.03 or 10% of AERONET AOTs.

3.9 Active Sensing (LITE, GLAS, CALIPSO)

Passive instruments have great difficulty with vertically resolving information about aerosols. However, space-borne lidars can provide a global view of the vertical structure of aerosol extinction from the Earth's surface through to the middle stratosphere, depending upon the presence of cloud and the aerosol density. Aerosol extinction from lidar measurements can be interpreted using the lidar equation. The single-scatter lidar equation is often written as:

$$P(R) = J\frac{c}{2}\frac{A}{R^2}\beta(R)T_{opt}T^2(R) \tag{6}$$

where *P(R)* is the instantaneous optical power returned from a sample volume at range *R*, *J* is the laser pulse energy, c is the speed of light, A is the receiver area, β is the volume backscatter cross section ($km^{-1}sr^{-1}$), and T_{opt} is the transmission of the lidar optics. The term $T^2(R)$ is the two-way transmission between the lidar and the sample volume and is given by:

$$T^2(R) = \exp\left[-2\int_0^R \sigma(z)\,dz\right] \tag{7}$$

where σ is the volume extinction coefficient, which includes the effects of both scattering and absorption. Then Eq. (7) is applicable to find the vertically distributed aerosol extinction.

The first spaceborne instrument, LITE, was a three-wavelength (1064, 532, and 256 nm) backscatter lidar developed by NASA and flown on the space shuttle Discovery for 10 days in September 1994 (McCormick et al. 1993; Winker et al. 1996). The LITE mission demonstrated that spaceborne lidar offers an effective means for detecting the spatial features of significant regional aerosol concentrations resulting, for example, from Saharan dust (Powell et al. 1997; Berthier et al. 2006), and African and South American biomass burning and anthropogenic sources (Grant et al. 1997; Hoff and Strawbridge 1997; Kent et al. 1998). The LITE mission stimulated the development of new space lidars such as the GLAS onboard ICESat (Spinhirne et al. 2005a, b) and the CALIPSO satellite which are currently generating aerosol products. The CALIPSO is flying in formation in a constellation of satellites called the A-Train. In addition to data from the A-train, CALIPSO data provides a more complete and understandable aerosol data set, which is used for various modeling studies.

3.10 Limb Sounding (SAGE, SAGE-2. POAM-2. POAM-3, HALOE, ILAS, SCIAMACHY)

The the Stratospheric Aerosol and Gas Experiment (SAGE) III instrument contains 12 spectral channels over the wavelength region of 0.28–1.54 μm and is essentially an improved version of its predecessors, SAGE I and II. The Naval Research Laboratory (NRL)'s the Polar Ozone and Aerosol Measurement (POAM) II onboard the French satellite SPOT-3 is a solar occultation instrument. It is designed as a simpler version of the SAGE II instrument to measure the vertical profiles of aerosols, O_3, NO_2, and H_2O in nine channels between 0.35 and 1.06 μm, with a 1 km vertical resolution (Glaccum et al. 1996). Aerosol products include the vertical profiles of polar region aerosols (Randall et al. 1996). Following a sensor improvement, the POAM III onboard the SPOT 4 satellite has been operational. NASA's HALOE instrument is able to measure vertical profiles of aerosol extinction. However, because it uses broadband and gas-filter radiometry methods (Russell et al. 1993) in the spectral range between 2.45 and 10.04 μm, it can provide stratospheric microphysical aerosol information when the aerosol loading is high, such as during volcanic eruptions (Hervig et al. 1998). Another occultation instrument called the Improved Limb Atmospheric Spectrometer (ILAS) can measure the vertical profiles of aerosol extinction in the infrared band between 6.21 and 11.77 μm and in a visible band centered near 0.78 μm. The SCanning Imaging Absorption spectroMeter for Atmospheric CHartographY (SCIAMCHY) instrument onboard EnviSAT is a high-resolution spectrometer designed to measure sunlight transmitted, reflected, and scattered by the Earth 's atmosphere or surface in the UV, visible, and NIR wavelength regions (0.24–2.38 μm, $\Delta\lambda = 0.24 \sim 1.48$ nm). It performs measurement not only in the limb but also in the nadir mode. Due to its wide wavelength range and spectral resolution, SCIAMACHY measurements turn out to be well-suited for the retrieval of atmospheric aerosol and have an uncertainty of 13∼20% (Nicolantonio et al. 2006). Additionally, SCIMAMCHY can provide UV-absorbing AI, which is similar to the TOMS AI (Graaf and Stammes 2005). The main problem of this instrument as related to the aerosol remote sensing is the large footprint (typically, $30\times60\,\mathrm{km}^2$). Therefore, the number of clear pixels is very limited.

3.11 Neural Network (AVHRR, OCTS, MODIS)

The neural network (NN) approach has been proven to be a useful tool to solve such nonlinear problems as the retrieval of aerosol from satellite radiance measurements. Li et al. (2001) used both a commercial NN package and multi-threshold techniques to identify smoke from biomass burning using AVHRR imagery data. NN can learn complex linear and nonlinear relationships in the radiometric data between smoke, clouds, and land. This method was applied to process daily AVHRR images acquired across Canada and the results showed reasonable correspondence with TOMS AI. Another NN technique is a LUT-based method. Okada et al. (2001) used a LUT-based NN technique for aerosol retrieval from OCTS/ADEOS data. In this method, LUTs storing TOA reflectance values with various atmosphere-ocean conditions are used for tuning the NN. Geometric conditions and reflectances at two ADEOS/OCTS bands (0.67 and 0.865 μm) are input into the NN, and aerosol properties are extracted. The NN technique has proven to reduce processing times, and is promising for effective aerosol retrievals on a global scale.

3.12 Multi-Sensor (GOME and ATSR2, SCIAMACHY and AATSR, MODIS, CALIPSO-CloudSat)

Given the unique information content of individual sensors, use of data from multiple sensors sheds a new light for aerosol remote sensing. Holzer-Popp et al. (2002a) proposed a synergetic aerosol retrieval method, called the Synergetic Aerosol Retrieval (SYNAER), which was applied to the combinations of GOME-ATSR2 onboard the ERS-2 satellite (Holzer-Popp et al. 2002a, b) and SCIAMACHY-AATSR onboard the EnviSAT (Holzer-Popp et al. 2008). The advantage of these combinations is that they provide complementary information from a radiometer and a spectrometer aboard one satellite platform to extract AOT and the most plausible aerosol type. The retrieval accuracy is 0.1 at three visible wavelengths (Holzer-Popp et al. 2002b).

Use of data from the same type of instrument but onboard different satellites is another approach. Tang et al. (2005) tested an aerosol retrieval method by exploiting the synergy between MODIS/Terra and MODIS/Aqua (SYNTAM) for various surface conditions including bright surfaces. Most recently, new techniques were proposed using active spaceborne LIDAR and passive radar measurements. Josset et al. (2008) showed a substantially improved accuracy of 1% bias and 0.07 standard deviation in aerosol retrievals over ocean by combining CALIPSO and CloudSat data.

4 Data Products and Applications

4.1 Operational Data Products

The successive satellite missions provide operational aerosol products based on state-of-art retrieval algorithms and users can easily acquire the data. Figures 3 and 4 show the global distributions of representative monthly-averaged aerosol products. Each product is used for aerosol monitoring separately or in combination. In the early days of aerosol monitoring, retrievals of aerosol properties from satellite data was only possible over oceans as shown in Fig. 3(a) and (b). However, the AOT is much larger near the continents than over oceans as shown in Fig. 4. This suggested that aerosol detection over land could be quite important so retrievals over land began in the 1980s. These efforts are well documented in several studies (e.g. Kaufman and Joseph 1982; Kaufman and Fraser 1983; Fraser et al. 1984; Herman et al. 1997; Kaufman et al. 1997; Torres et al. 1998; Veefkind and Leeuw 1998; Knapp 2002; Knapp and Stowe 2002; Knapp et al. 2002; von Hoyningen et al. 2003; Hsu et al. 2004; Remer et al. 2005; Levy et al. 2007a). The development of aerosol retrieval algorithms over

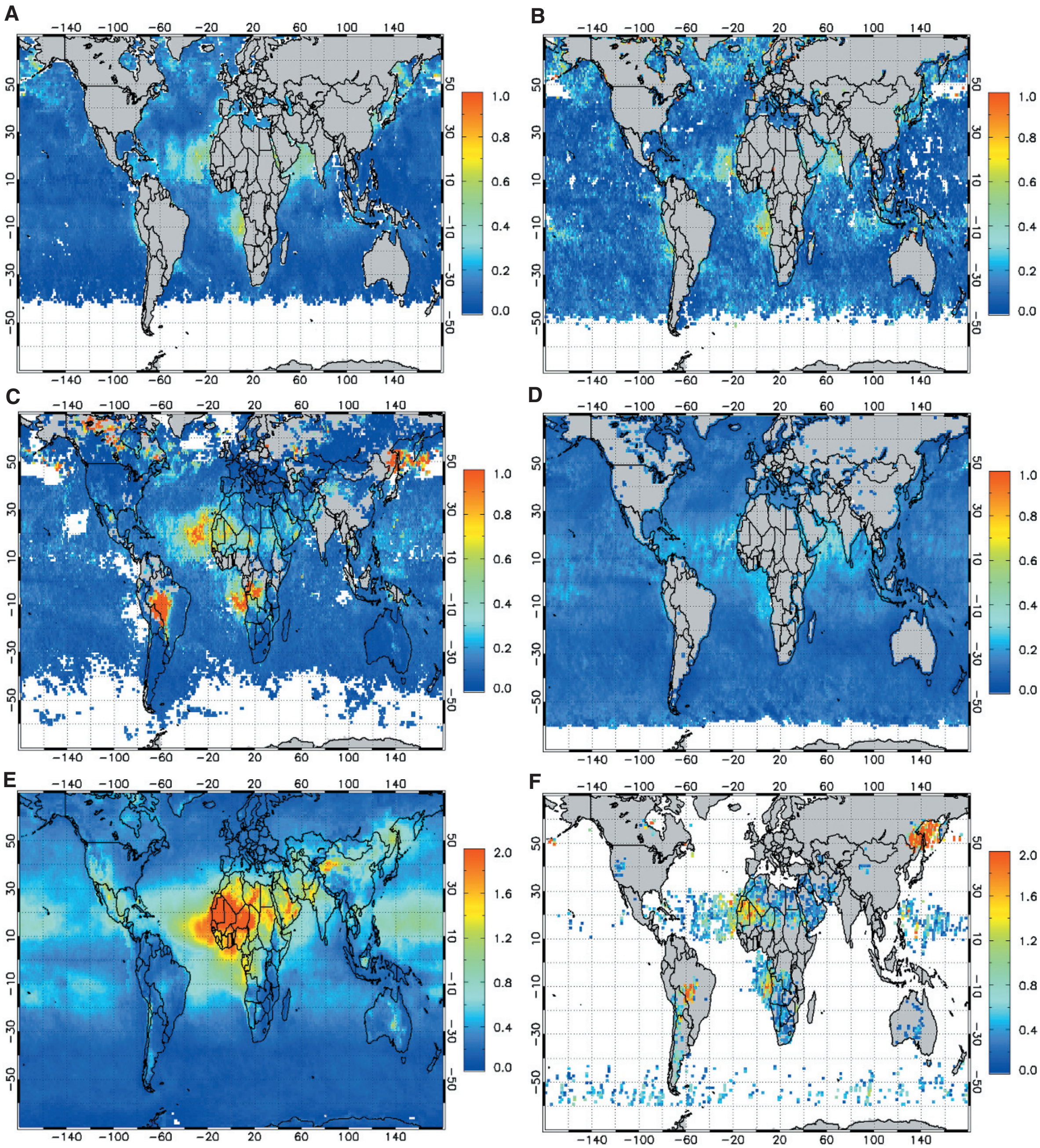

Fig. 3 Monthly-averaged aerosol products for August 1998 before Terra

land and the interest in aerosol monitoring research has accelerated since the launch of Terra in 1999. The first and the second generations of satellite aerosol monitoring can be distinguished before and after the launch of Terra.

In Figs. 3 and 4, large AOTs are generally shown to the west of the middle and northern parts of Africa and the Asian continent, and are mainly due to desert dust, biomass burning, and man-made pollution. The AOTs over the eastern and western coasts of North America are also mainly due to man-made pollution. Biomass burning in South America and southern Africa are the main sources of carbonaceous aerosols. The general spatial distribution pattern looks similar in all retrievals but significant differences among the sensors still exist due to various reasons: sensor calibration, aerosol model assumptions, cloud screening, treatment of surface reflectance, among others.

4.2 Inter-Comparisons

Algorithms for aerosol retrievals are sensor-specific because of the different characteristics of the satellite instruments. Moreover, different types and versions of the aerosol retrieval algorithms have been developed for the same instrument. When applied to the same data

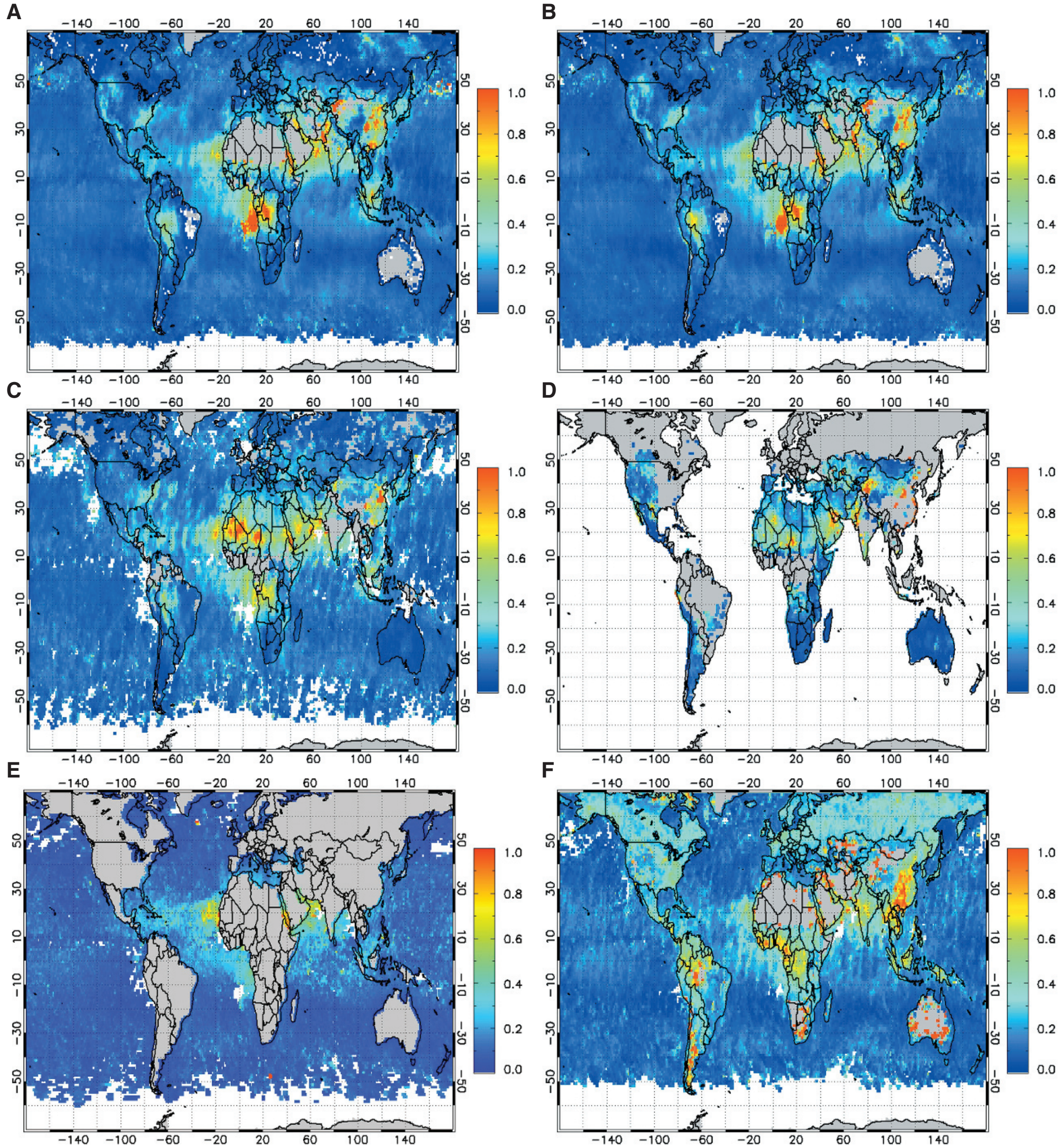

Fig. 4 Monthly-averaged aerosol products for August 2006 after Terra

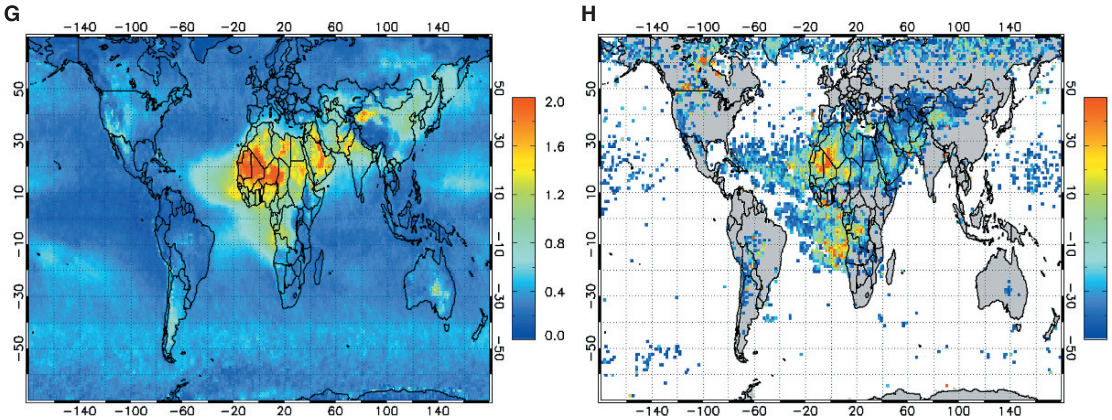

Fig. 4 (continued)

set, they yield rather different results. This can be confusing to users of the products and policy makers, with damaging consequences.

Abdou et al. (2005) showed comparisons between AOTs retrieved by the MODIS and by MISR to explore the similarities and differences between them. They showed that over land, MODIS AOTs at 470 and 660 nm are larger than MISR AOTs by about 35 and 10%, on average. Over oceans, MISR AODs at 470 and 660 nm are generally higher than MODIS AOTs by about 0.1 and 0.05, respectively. In Myhre et al. (2004), an 8-month period of AOTs derived from five different retrieval algorithms applied to 4 satellite instruments, such as AVHRR, OCTS, POLDER, and TOMS, are compared. There is at least a factor of 2 differences between the AOTs from these retrievals. In Fig. 5, the largest uncertainties are found in the Southern Hemisphere and the smallest differences are mostly located near the continents in the Northern Hemisphere. Differences in cloud screening techniques may account for the large discrepancy.

The monthly mean AOTs over oceans from a total of 9 aerosol retrievals during a period of 40 months (September 1997–December 2000) was made by Myhre et al. (2005). In most ocean regions, significant differences in AOT were identified. Figure 6 shows the zonal mean AOT for the entire 40-month period (a), the 8-month period from January to August 1998 (b), and the 10-month period from March to December 2000 (c). In this figure, the largest differences are found at high latitudes and the largest differences between MODIS and MISR are also found at high latitudes. For the entire period, the differences are largest in the southern hemisphere; during the period of March–December 2000, large differences are also found in the northern hemisphere.

Inter-comparisons between the long-term (1983–2000) aerosol products from AVHRR and TOMS are discussed in Jeong and Li (2005). In general, each product is complimentary to the other in terms of global aerosol distribution. However, the AVHRR cannot represent continental sources except for large aerosol plumes. The TOMS AI and AOT have differences in where higher aerosol loading over land are located. These differences may arise from inherent problems found in aerosol retrievals, such as cloud, ocean color contamination, and induced oceanic aerosols. Figure 7 shows a common problem originated from cloud screening in AVHRR aerosol retrieval. The choice of aerosol size distribution is another problematic issue. Jeong et al. (2005) demonstrated that the considerable discrepancies between the AVHRR and MODIS AOTs are attributed to differences in aerosol size distribution functions used in the retrievals, namely, the power law (AVHRR) and bimodal log normal (MODIS) size distribution functions (Fig. 8).

Kokhanovsky et al. (2007) provided the first brief discussion concerning an inter-comparison study of AOT at 0.55 μm retrieved using six different satellite instruments and ten different algorithms for a single scene over central Europe on October 13, 2005. The spatially averaged AOT was equal to 0.14 for MISR, NASA MODIS and POLDER products and is smaller by 0.01 for the ESA MERIS and larger by 0.04 for the MERIS BAER product. The AOT from AATSR

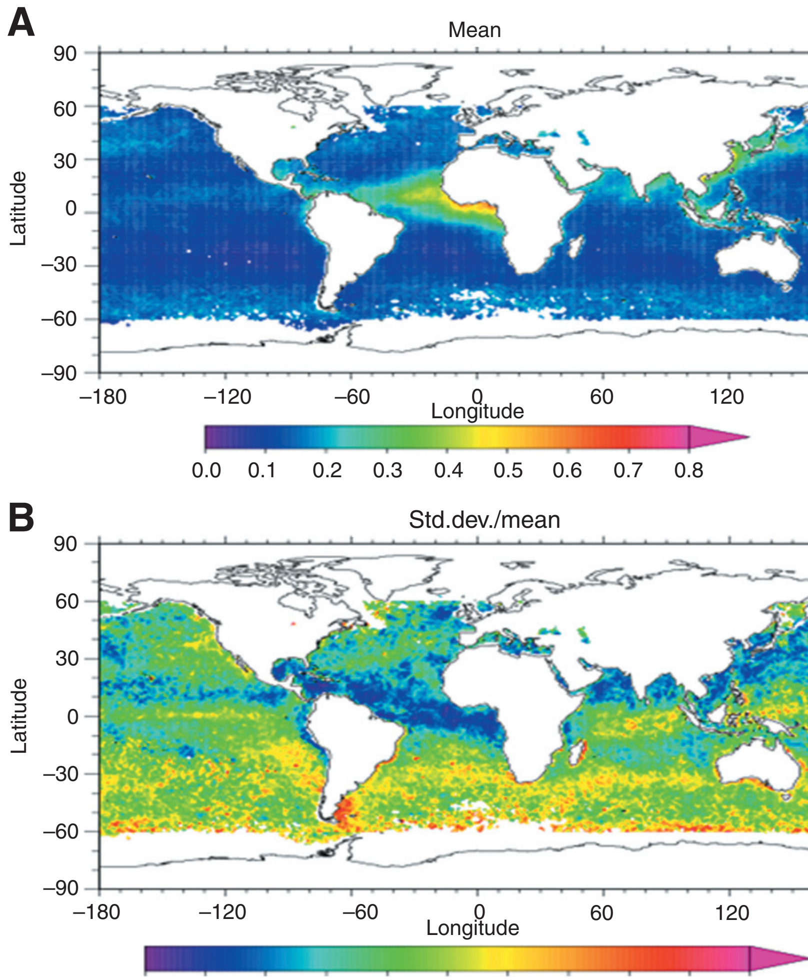

Fig. 5 Averaged statistics for the five aerosol retrievals from November 1996 to June 1997: (**a**) mean and (**b**) standard (after Myhre et al. 2004)

gives on average larger values than those from all other instruments, while SCIAMACHY retrievals underestimate aerosol loading. In Fig. 9, validation against AERONET shows that MERIS provides the most accurate AOT retrievals for this scene.

4.3 Aerosol Climatology

The longest climatology of AOT is generated from AVHRR using the two-channel retrieval algorithm for the period extending from August 1981 to June 2005 (Mishchenko et al. 2007a, b). A slightly decreasing trend in AOT is seen over this time period (Fig. 10). Analyses of regional trends reveal decreases over Europe, part of the Atlantic Ocean, and increases along a portion of the western coast of Africa, along the southern and south-east coasts of Asia, and over the 45–60°S latitudinal belt (Mishchenko et al. 2007b). An unsurprising result is that the northern hemispheric mean AOT systematically exceeds that averaged over the southern hemisphere. The effects of two major volcanic eruptions (El Chichon and Mt. Pinatubo) are clearly visible, consistent with the SAGE stratospheric AOT. Bauman et al. (2003a, b) used data from SAGE II and CLAES during December 1984–August 1999 to develop stratospheric aerosol climatology. They found that it took 5 years after the Mt. Pinatubo eruption for the stratospheric aerosol loading to return to its pre-eruption level.

4.4 Synergy

A number of satellite-derived aerosol products are available, and the synergy among these satellite

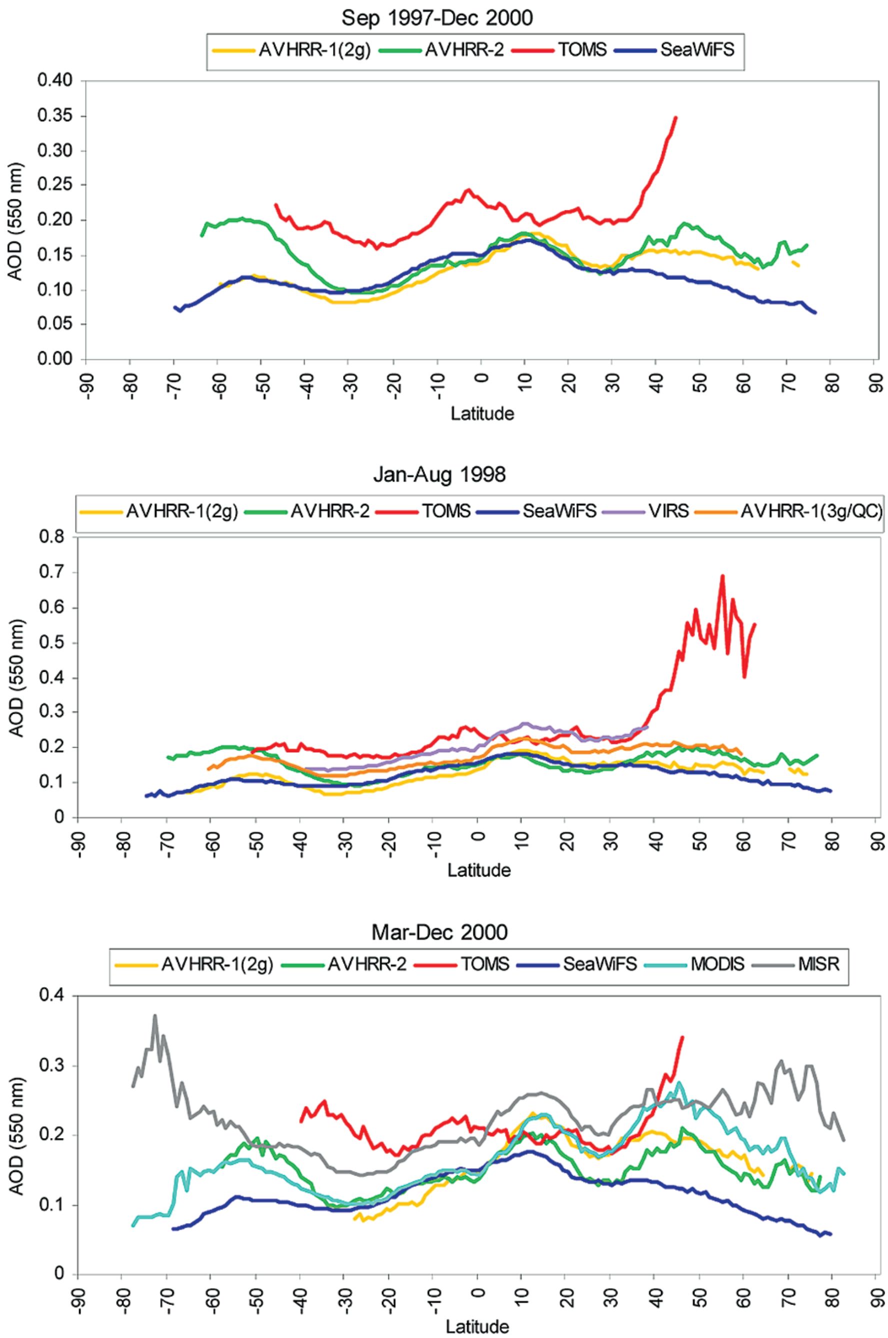

Fig. 6 Zonal mean AOT as a function of latitude for the entire period of investigation, as well as for two selected periods (after Myhre et al. 2004)

products may lead to a new and improved data set. Global aerosol products from satellites such as AVHRR, TOMS, and MODIS are particularly useful in this regard. The spatial distributions of the aerosol products from these instruments are complimentary in revealing different aspects of aerosol characteristics. For example, aerosol SSAs can be derived from the combination of AOT and AI (Hu et al. 2007) and a combination of satellite and ground-based measurements (Lee et al. 2007b). Aerosol type classification by absorption and Ångström exponent was first suggested by Higurashi and Nakajima (2002). Improved aerosol type classification methods by merging essential information about aerosol mass loading from AOT,

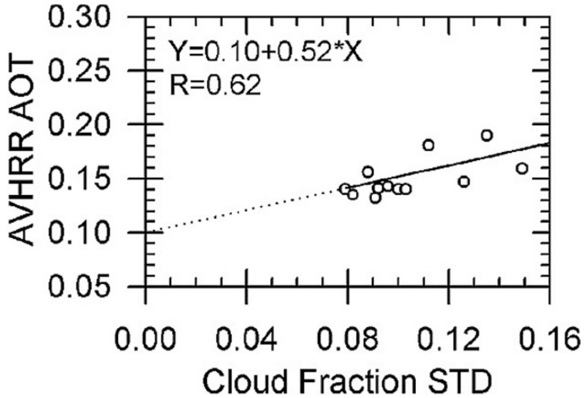

Fig. 7 AOT as a function of standard deviation (STD) of the ISCCP cloud fraction over the coastal areas of Peru and Chile (10–30°S, 70–90°W) where a region of enhanced AVHRR AOT is shown (after Jeong and Li 2005). The cloud fraction STD was found to be positively correlated with the AVHRR AOT with a correlation coefficient equal to 0.62

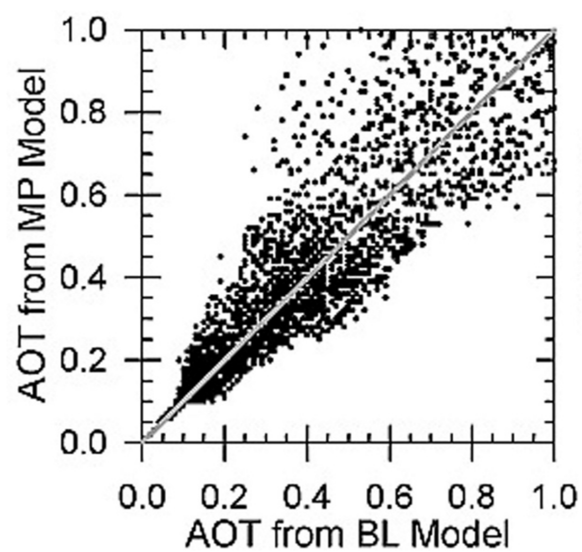

Fig. 8 Scatterplot of AOT from the modified power law models versus that from bimodal lognormal models (after Jeong et al. 2005). Note that they exhibit very large discrepancies by up to a factor of two. This suggests that the selection of a particular aerosol model is an important factor influencing the retrieval of the AOT

size from Ångström or fine mode fraction, and absorption by AI were developed (Barnaba and Gobbi 2004; Jeong and Li 2005; Lee et al. 2006c; Kim et al. 2007). Finally, the synergy between different products from the same instrument can overcome some of the limitations of surface monitoring networks and enhance daily air quality forecasts associated with particle pollution as shown in Fig. 11 (Al-Saadi et al. 2005).

5 Future Instruments

5.1 APS/GLORY

The Aerosol Polarimetry Sensor (APS) onboard the Glory satellite (http://glory.gsfc.nasa.gov/index.html) is scheduled for launch into a low Earth orbit (LEO) in December 2008 (Mishchenko et al. 2007c). The APS is designed to measure the properties of aerosols for the long-term effects on the Earth climate record and it will enable a greater understanding of the seasonal variability of aerosol properties. The APS has the ability to collect multi-angle, multi-spectral photopolarimetric measurements of the atmosphere and the underlying surface along the satellite ground track. APS observations will provide accurate retrievals of aerosol microphysical parameters and are expected to improve global aerosol assessments.

5.2 NPP

The National Polar-orbiting Operational Environmental Satellite System Preparatory Project (NPP) is a joint mission with the NPOESS Integrated Program Office (IPO) (http://jointmission.gsfc.nasa.gov/). The NPP will provide continuity in global Earth Science observations of the atmosphere, land, and oceans after the EOS Terra and Aqua missions are over. NPP will take measurements of atmospheric and SST, humidity soundings, land and ocean biological productivity, and cloud and aerosol properties using three different sensors: the Visible Infrared Imaging Spectroradiometer Suite (VIIRS), the Crosstrack Infrared Sounder (CrIS), and the Advanced Technology Microwave Sounder (ATMS). The launch is planned for September 2009, with a mission duration of 5 years.

5.3 EarthCARE

The Earth Clouds, Aerosols, and Radiation Explorer (EarthCARE), due for launch in 2012 (ESA 2004), is a joint European-Japanese mission addressing the need for a better understanding of the interactions between cloud, radiative and aerosol processes that play a role in climate regulation. Four distinct instruments are planned for deployment on EarthCARE:

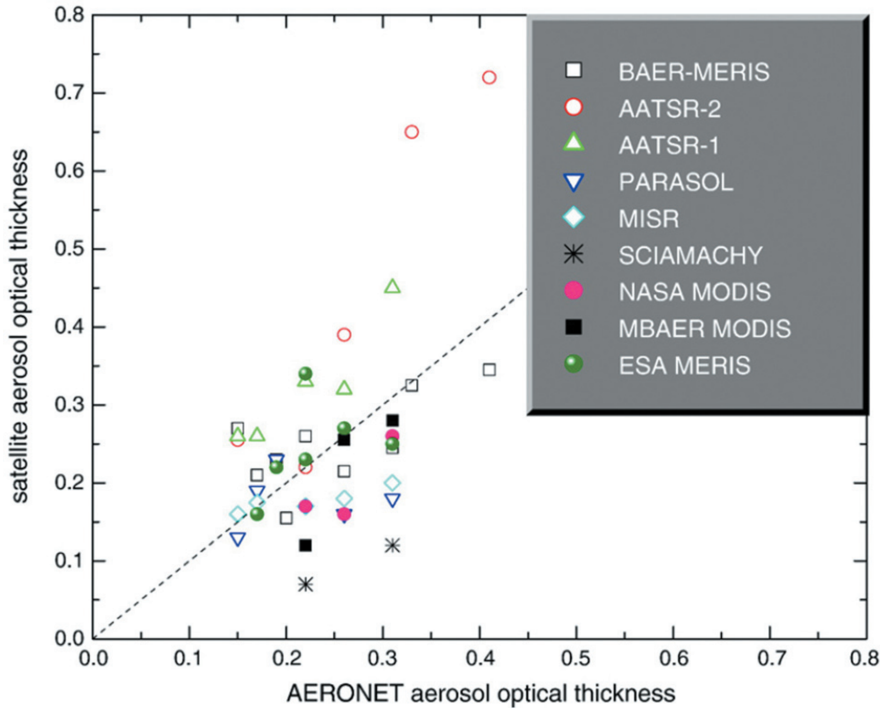

Fig. 9 Comparison of satellite and ground measurements of AOT at 0.55 µm (after Kokhanovsky et al. 2007)

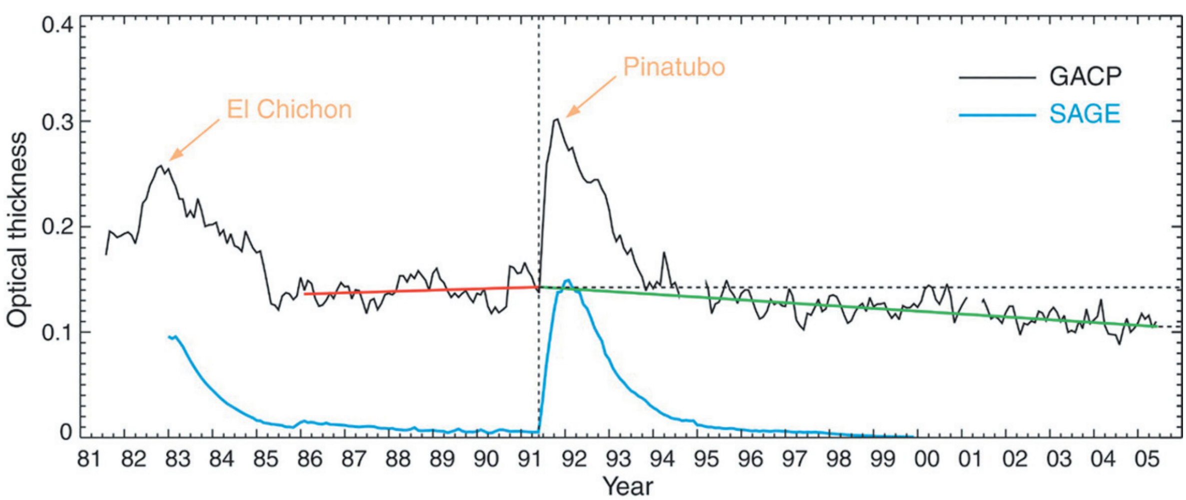

Fig. 10 Time series of the globally-averaged column AOT over the oceans and the SAGE record of globally-averaged stratospheric AOT (after Mishchenko et al. 2007a)

the Backscatter Lidar (ATLID), the Cloud Profiling Radar (CPR), the Multi-Spectral Imager (MSI), and the Broadband Radiometer (BBR). The goal of this mission is to improve the representation and understanding of the Earth's radiative balance in climate and numerical weather forecast models by acquiring vertical profiles of clouds and aerosols, as well as the radiances at the top of the atmosphere.

5.4 MSI/Sentinel-2

Sentinel-2 is the medium spatial resolution optical mission of the Global Monitoring for Environment and Security (GMES) program (http://www.esa.int/esapub/bulletin/bulletin131/bul131b_martimort.pdf). The multi-spectral instrument (MSI) will gen-

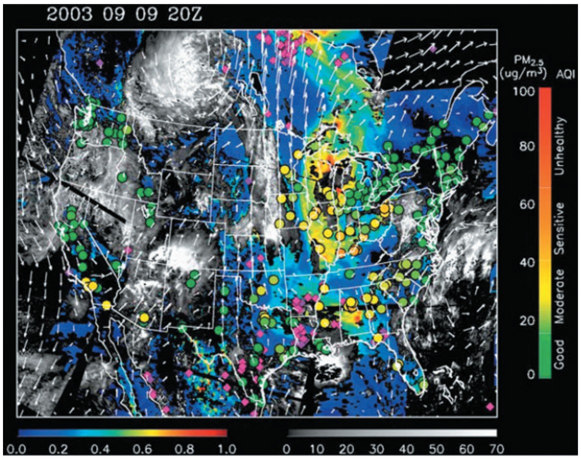

Fig. 11 Example of an air quality forecast (after Al-Saddi et al. 2005). The colored and *white-black* contour areas represent MODIS AOT and cloud. Continuous PM2.5 monitoring stations are shown as a circle color-coded by the hourly concentration [scale on the right, with associated AQI (EPA 1999)]. Fire locations are shown as diamonds and color-coded according to the fire probability: *bright pink* for higher probability fires and *violet* for lower probability fires. The 850 mb wind direction and speed from the NCEP Eta Model are shown as *white* vectors

erate optical images in 13 spectral channels in the visible and short-wave infrared range (443–2190 nm) down to 10, 20, and 60 m spatial resolution with an image width of 290 km. The MSI features a three-mirror anastigmat (TMA) telescope with a pupil diameter of about 150 mm; it is the key to the high image quality across the wide field of view (290 km). The telescope structure and mirrors are made of silicon carbide to minimize thermal deformation. The launch of the first Sentinel-2 satellite is planned for 2012.

5.5 Sentinel-3

Another GMES satellite, the Sentinel-3, will continue EnviSAT's mission and includes enhancements to meet the operational revisit requirements and to facilitate new products and evolution of services (http://www.esa.int/esapub/bulletin/bulletin131/bul131c_aguirre.pdf). The two optical instruments, Ocean and Land Colour Instrument (OLCI) based on MERIS/EnviSAT and The Sea and Land Surface Temperature Radiometer (SLSTR) based on AATSR/EnviSAT, will provide a common quasi-simultaneous view of the Earth to help develop synergetic products. The first launch is expected in 2011/2012.

5.6 TRAQ

The Tropospheric composition and Air Quality (TRAQ) is a mission focused on understanding the tropospheric system for air quality, sources and sinks, and climate change (Levelt et al. 2006). New synergistic sensors include a UV/VIS/NIR/SWIR instrument (TROPOMI), which is a follow-on instrument to OMI, an FTIR instrument (SIFTI), a cloud detector (CLIM) and an instrument resembling POLDER (OCAPI), which will extend the spectral range up to 2.2 μm for pollution aerosol detection. The TRAQ mission will be the first mission fully dedicated to air quality and the science issues concerning tropospheric composition and global change.

6 Summary

Since its beginning three decades ago, satellite remote sensing of atmospheric aerosols offers more complete spatial coverage and includes vertical profile and spectral/optical information when compared to the point-measurement data typically used to evaluate local-scale aerosols. Operational satellite aerosol products such as AOT, Ångström exponent, mode fraction, single scattering albedo, and the vertical profile are currently available from space agencies such as NOAA, NASA, ESA, CNES, KNMI, JAXA, etc. Several aerosol retrieval algorithms for specific sensor characteristics are reviewed. The independent satellite measurements can be use to study the spatial distribution, transport, origin, and climatology of aerosols. A combination of satellite measurements can be used to examine their compatibility and synergy for producing improved products. Satellite data can also be used for air quality forecasting. These efforts will be base of future satellite missions.

Acknowledgments The authors are grateful to the many agencies that have providing the satellite data used here. They include PATMOS data from NESDIS/NOAA, POLDER/PARASOL data from the ICARE thematic center, AVHRR data from GISS/NASA, MODIS data from NASA's LAADS Web, MISR from ASDC/NASA, GOME and SCIAMACHY data from KNMI's TEMIS, SeaWiFS data from GSFC/NASA's ocean color web and TOMS data from GSFC/NASA.

Abbreviations

AATSR	Advance Along Track Scanning Radiometer
ACE	Aerosol Characterization Experiments
AERONET	Aerosol Robotic Network
AI	Aerosol Index
AOD	Aerosol Optical Depth
AOT	Aerosol Optical Thickness
APS	Aerosol Polarimetry Sensor
AQI	Air Quality Index
ATBD	Algorithm Theoretical Basis Document
ATMS	Advanced Technology Microwave Sounder
AVHRR	Advanced Very High Resolution Radiometer
BAER	Bremen Aerosol Retrieval
BBR	Broadband Radiometer
BRF	Bidirectional Reflectance Factor
CALIPSO	Cloud-Aerosol Lidar and Infrared Pathfinder Satellite Observations
CHRIS	Compact High Resolution Imaging Spectrometer
CNES	le Centre National d'Etudes Spatiales
CPR	Cloud Profiling Radar
CrIS	Crosstrack Infrared Sounder
DDV	Dense Dark Vegetation
DLR	German Aerospace Centre
EarthCARE	Earth Clouds, Aerosols, and Radiation Explorer
ENVISAT	Environment Satellite (http://envisat.esa.int)
EOS	Earth Observation System
ERS	European Remote Sensing satellite
ERTS	Earth Resoureces Technology Satellite
ESA	European Space Agency (http://www.esa.it/export/esaCP/index.html)
FMF	Fine Mode Fraction
GACP	Global Aerosol Climatology Product
GLAS	Geoscience Laser Altimeter System
GMES	Global Monitoring for Environment and Security
GMS	Geostationary Meteorology Satellite
IGAC	International Global Atmospheric Chemistry Observation
ILAS	Improved Limb Atmospheric Spectrometer
ISCCP	International Satellite Cloud Climatology Project
JAXA	Japan Aerospace Exploration Agency
JPL	Jet Propulsion Laboratory
KNMI	Royal Netherlands Meteorological Institute
L1, L2	Level 1, Level 2
LEO	Low Earth Orbit
LER	Lambert Equivalent Reflectivity
LIDAR	Light Detection and Ranging
LITE	Lidar In-space Technology Experiment
LUT	Look Up Table
MERIS	Medium Resolution Imaging Spectrometer Instrument
MISR	Multiangle Imaging SpectroRadiometer
MODIS	Moderate Resolution Imaging Spectroradiometer
MSI	Multi-Spectral Imager
NASA	National Aeronautics and Space Administration
NIR	Near InfraRed
NN	Neural Network
NOAA	the National Ocean and Atmosphere Administration
NPP	National Polar-orbiting Operational Environmental Satellite System Preparatory Project
NRL	Naval Research Laboratory
PATMOS	Pathfinder Atmosphere
POAM	Polar Ozone and Aerosol Measurement
POLDER	POLarization and Directionality of the Earth's Reflectances
PROBA	Project for On-Board Autonomy
ROD	Rayleigh optical depth
SAM	Stratospheric Aerosol Measurement
SCIAMACHY	SCanning Imaging Absorption 5 spectroMeter for Atmospheric CHartographY

SeaWiFS	Sea-viewing Wide Field-of-view Sensor
SLSTR	Sea and Land Surface Temperature Radiometer
SPOT	Satellite Pour l'Observation de la Terre
SSA	Single Scattering Albedo
SSD	Space Shuttle Discovery
SST	Sea Surface Temperature
SWIR	Short Wave Infra Red
SYNAER	Synergetic Aerosol Retrieval
SYNTAM	Synergy a combination of MODIS/Terra and MODIS/Aqua
TARFOX	the Tropospheric Aerosol Radiation Forcing Experiment
TIR	Thermal InfraRed
TMA	three-mirror anastigmat
TOA	Top of Atmosphere
TOMS	Total Ozone Mapping Spectrometer
TRAQ	Tropospheric composition and Air Quality
UV	Ultra Violet
VI	Vegetation Index
VIIRS	Visual/Infrared Imager Radiometer Suite
VIRS	Visualisation and analysis tool
VNIR	Visible Near Infrared

References

Abdou WA, DJ Diner, JV Martonchik, CJ Bruegge, RA Kahn, BJ Gaitley, KA Crean, LA Remer, and B Holben (2005) Comparison of coincident MISR and MODIS aerosol optical depths over land and ocean scenes containing AERONET sites. *J. Geophys. Res.* doi:10.1029/2004JD004693.

Al-Saadi J, J Szykman, B Pierce, C Kittaka, D Neil, DA Chu, L Remer, L Gumley, E Prins, L Weinstock, C McDonald, R Wayland, and F Dimmick (2005) Improving national air quality forecasts with satellite aerosol observations. *Bull. Am. Met. Soc.* 86(9): 1249–1261.

Barnaba F and GP Gobbi (2004) Aerosol seasonal variability over the Mediterranean region and relative impact of maritime, continental and Saharan dust particles over the basin from MODIS data in the year 2001. *Atmos. Chem. Phys*. 4: 2367–2391.

Barnsley M, J Settle, M Cutter, D Lobb, and F Teston (2004) The PROBA/CHRIS mission: A low-cost smallsat for hyperspectral, multi-angle, observations of the earth surface and atmosphere. *IEEE Trans. Geosci. Remote Sens.* 42: 1512–1520.

Bates TS, BJ Huebert, JL Gras, FB Griffiths, and PA Durkee (1998) International Global Atmospheric Chemistry (IGAC) Project's First Aerosol Characterization Experiment (ACE 1): Overview. *J. Geophys. Res. 103*(D13): 16297–16318.

Bauman JJ, PB Russell, MA Geller, and P Hamill (2003a) A stratospheric aerosol climatology from SAGE II and CLAES measurements: 1. Methodology. *J. Geophys. Res.* 108(D13), doi:10.1029/2002JD002992.

Bauman JJ, PB Russell, MA Geller, and P Hamill (2003b) A stratospheric aerosol climatology from SAGE II and CLAES measurements: 2. Results and comparisons, 1984–1999. *J. Geophys. Res.* 108(D13): 4383, doi:10.1029/2002JD002993.

Berthier S, P Chazette, P Couvert, J Pelon, F Dulac, F Thieuleux, C Moulin, and T Pain (2006) Desert dust aerosol columnar properties over ocean and continental Africa from Lidar in-Space Technology Experiment (LITE) and Meteosat synergy. *J. Geophys. Res.* 111(D21202), doi:10.1029/2005JD006999.

Bourassa AE, DA Degenstein, RL Gattinger, and EJ Llewellyn (2007) Stratospheric aerosol retrieval with optical spectrograph and infrared imaging system limb scatter measurements. *J. Geophys. Res*. 112(D10217), doi:10.1029/2006JD008079.

Breon FM, D Tanre, and S Generoso (2002) Aerosol effect on cloud droplet size monitored from satellite. *Science.* 295: 834–838.

Christopher SA and J Wang (2004) Intercomparison between multi-angle imaging spectroradiometer (MISR) and sunphotometer aerosol optical thickness in dust source regions over China: Implications for satellite aerosol retrievals and radiative forcing calculations. *Tellus.* B56(5): 451–456, doi:10.1111/j.1600-0889.2004.00120.

Chu DA, YJ Kaufman, C Ichoku, LA Remer, D. Tanré, and BN Holben (2002) Validation of MODIS aerosol optical depth retrieval overland. *Geophys. Res. Lett.* 29, doi:10.1029/2001GL013205.

Chu WP and MP McCormick (1979) Inversion of stratospheric aerosol and gaseous constituents from spacecraft solar extinction data in the 0.38–1.0-Mum wavelength region. *Appl. Opt*. 18: 1404–1413.

Chu WP, MP McCormick, J Lenoble, C Brognoiz, and P Pruvost (1989) SAGE II inversion algorithm. *J. Geophys. Res.* 94: 8339–8351.

Costa MJ, BJ Sohn, V Levizzani, AM Silva (2006) Radiative forcing of Asian dust determined from the synergized GOME and GMS satellite data – A case study. *J. Meteorol. Soc. Jpn.* 84: 85–95.

Dave J (1973) Development of the programs for computing characteristics of ultraviolet radiation: Scalar case. NAS5-21680, NASA Goddard Space Flight Cent., Greenbelt, Md.

Davidson CI, RF Phalen, PA Solomon (2005) Airborne particulate matter and human health: A review. *Aerosol Sci. Technol.* 39(8): 737–749.

Deuzé JL, M Herman, P Goloub, D Tanré, and A Marchand (1999) Characterization of aerosols over ocean from POLDER/ADEOS-1. *Geophys. Res. Lett. 26*(10): 1421–1424.

Diner DJ, WA Abdou, TP Ackerman, K Crean, HR Gordon, RA Kahn, JV Martonchik, S McMuldroch, SR Paradise, B Pinty, MM Verstraete, M Wang, and RA West (2008) MISR level 2 aerosol retrieval algorithm theoretical basis. Jet Propul. Lab. Pasadena, CA, JPL-D 11400, Rev. G.

Diner DJ, WA Abdou, CJ Bruegge, JE Conel, KA Crean, BJ Gaitley, MC Helmlinger, RA Kahn, JV Martonchik, SH Pilorz, and BN Holben (2001) MISR aerosol optical depth retrievals over southern Africa during the SAFARI-2000 dry season campaign. *Geophys. Res. Lett*. 28: 3127–3130.

Diner DJ, JC Beckert, TH Reilly, CJ Bruegge, JE Conel, RA Kahn, JV Martonchik, TP Ackerman, R Davies, SAW Gerstl, HR Gordon, JP Muller, RB Myneni, PJ Sellers, B Pinty, and MM Vertraete (1998) Multi-angle Imaging Spectro Radiometer (MISR) instrument description and experiment overview. *IEEE Trans. Geosci. Remote Sens.* 36: 1072–1087.

Dulac F, S Tanré, G Bergametti, P Buat-Ménard, M Desbois, and D Sutton (1992) Assessment of the African airborne dust mass over the western Mediterranean Sea using Meteosat data. *J. Geophys. Res.* 97: 2489–2506.

Durkee PA, DR Jensen, EE Hindman, and TH Vonder Haar (1986) The relationship between marine aerosols and satellite detected radiance. *J. Geophys. Res.* 91: 4063–4072.

EPA (1999) Guideline for reporting of daily air quality – air quality index (AQI). EPA-454/R-99-010, 25 pp. [Available online at http://www.epa.gov/ttn/ oarpg/t1/memoranda/rg701.pdf.]

European Space Agency (ESA) (2004) Reports for mission selection, The six candidate earth explorer missions: EarthCARE. ESA SP-1279(1).

Fraser RS (1976) Satellite measurement of mass of Sahara dust in the atmosphere. *Appl. Opt.* 15: 2471–2479.

Fraser RS, YJ Kaufman, and RL Mahoney (1984) Satellite measurements of aerosol mass and transport. *Atmos. Environ*. 18: 2577–2584.

Froidevaux L and A Douglass (2001) Earth Observing System (EOS) aura science data validation plan (available from http://eos-aura.gsfc.nasa.gov/mission/validation.html).

Geogdzhayev IV, MI Mishchenko, WB Rossow, B Cairns, and AA Lacis (2002) Global two-channel AVHRR retrievals of aerosol properties over the ocean for the period of NOAA-9 observations and preliminary retrievals using NOAA-7 and NOAA-11 data. *J. Atmos Sci.* 59: 262–278.

Glaccum W, R Lucke, RM Bevilacqua, EP Shettle, JS Hornstein, DT Chen, JD Lumpe, SS Krigman, DJ Debrestian, MD Fromm, F Dalaudier, E Chassefiere, C Deniel, CE Randall, DW Rusch, JJ Olivero, C Brogniez, J Lenoble, and R Kremer (1996) The polar ozone and aerosol measurement instrument. *J. Geophys. Res.* 101: 14479–14487.

Goloub P, D Tanré, JL Deuzé, M Herman, A Marchand, and FM Bréon (1999) Validation of the first algorithm for deriving the aerosol properties over the ocean using the POLDER/ADEOS measurements. *IEEE Trans. Geosci. Remote Sens.* 37(3): 1586–1596.

Gordon HR and AY Morel (1983) Remote Assessment of Ocean Color for Interpretation of Satellite Visible Imagery: A Review. Springer-Verlag, New York.

Gordon HR and M Wang (1994) Retrieval of water-leaving radiance and aerosol optical thickness over the oceans with SeaWiFS: A preliminary algorithm. *Appl. Opt.* 33: 443–452.

Graaf M de and P Stammes (2005) SCIAMACHY absorbing aerosol index – calibration issues and global results from 2002–2004. *Atmos. Chem. Phys*. 5: 2385–2394, SRef-ID:1680-7324/acp/2005-5-2385.

Grant WB, EV Browell, CF Butler, and GD Nowicki (1997) LITE measurements of biomass burning aerosols and comparisons with correlative airborne lidar measurements of multiple scattering in the planetary boundary layer. In: A Ansmann, R Neuber, P Rairoux, and U Wandinger (eds) *Advances in Atmospheric Remote Sensing with Lidar.* Springer-Verlag, Berlin, 153–156.

Grey WMF, PRJ North, and SO Los (2006) Computationally efficient method for retrieving aerosol optical depth from ATSR-2 and AATSR data. *Appl. Opt*. 45: 2786–2795.

Griggs M (1975) Measurements of atmospheric aerosol optical thickness over water using ERTS-1 data. *J. Air Pollut. Control. Assoc.* 25: 622–626.

Gu YY, CS Gardner, PA Castelberg, GC Papen, and MC Kelley (1997) Validation of the Lidar In-space Technology Experiment: Stratospheric temperature and aerosol measurements. *Appl. Opt.* 36: 5148–5157.

Hale GM, and MR Querry (1973) Optical constants of water in the 200 nm to 200 μm wavelength region. *Appl. Opt*. 12: 555–563.

Herman JR, PK Bhartia, O Torres, C Hsu, C Seftor, and E Celarier (1997) Global distribution of UV-absorbing aerosols from Nimbus 7/TOMS data. *J. Geophys. Res.* 102: 16911–16922.

Herman M, JL Deuzé, C Devaux, Ph Goloub, FM Bréon, and D Tanré (1997) Remote sensing of aerosols over land surfaces, including polarization measurements; application to some airborne POLDER measurements. *J. Geophys. Res.* 102: 17039–17049.

Hervig ME, T Deshler, and JM Russell III (1998) Aerosol size distributions obtained from HALOE spectral extinction measurements. *J. Geophys. Res.* 103: 1573–1583.

Higurashi A and T Nakajima (1999) Development of a two channel aerosol retrieval algorithm on global scale using NOAA AVHRR. *J. Atmos. Sci.* 56: 924–941.

Higurashi A and T Nakajima (2002) Detection of aerosol types over the East China Sea near Japan from four-channel satellite data. *Geophys. Res. Lett. 29*(17): 1836, doi:10.1029/2002GL015357.

Hoff RM and KB Strawbridge (1997) LITE observations of anthropogenically produced aerosols. In: A Ansmann, R Neuber, P Rairoux, and U Wandinger (eds) *Advances in Atmospheric Remote Sensing with Lidar*, Springer-Verlag, Berlin, 145–148.

Holzer-Popp T, M Schroedter-Homscheidt, H Breitkreuz, L Klüser, D Martynenko (2008) Synergistic aerosol retrieval from SCIAMACHY and AATSR onboard ENVISAT. *Atmos. Chem. Phys. Discuss.* 8: 1–49.

Holzer-Popp T, M Schroedter, and G Gesell (2002a) Retrieving aerosol optical depth and type in the boundary layer over land and ocean from simultaneous GOME spectrometer and ATSR-2 radiometer measurements, 1, Method description. *J. Geophys. Res.* 107(D21): 4578, doi:10.1029/2001JD002013.

Holzer-Popp T, M Schroedter, and G Gesell (2002b) Retrieving aerosol optical depth and type in the boundary layer over land and ocean from simultaneous GOME spectrometer and ATSR-2 radiometer measurements, 2, Case study application and validation. *J. Geophys. Res.* 107(D24): 4770, doi:10.1029/2002JD002777.

Hsu NC, JR Herman, PK Bhartia, CJ Seftor, O Torres, AM Thompson, JF Gleason, TF Eck, and BN Holben (1996) Detection of Biomass Burning Smoke from TOMS Measurements. *Geophys. Res. Lett*. 23(7): 745–748.

Hsu NC, JR Herman, O Torres, BN Holben, D Tanré, TF Eck, A Smirnov, B Chatenet, and F Lavenu (1999) Comparison of the TOMS aerosol Index with Sun-photometer aerosol optical thickness: Results and application. *J. Geophy. Res.* 23: 745–748.

Hsu NC, SC Tsay, MD King, and JR Herman (2004) Aerosol properties over bright-reflecting source regions. *IEEE Trans. Geosci. Remote Sens.* 42(3): 557–569.

Hsu NC, SC Tsay, MD King, and JR Herman (2006) Deep blue retrievals of Asian aerosol properties during ACE-Asia. *IEEE Trans. Geosci. Remote Sens.* 44: 3180–3195.

Hu RM, RV Martin, and TD Fairlie (2007) Global retrieval of columnar aerosol single scattering albedo from space-based observations. *J. Geophys. Res.* 112(D02204), doi:10.1029/2005JD006832.

Huebert BJ, T Bates, PB Russell, G Shi, YJ Kim, K Kawamura, G Carmichael, and T Nakajima (2003) An overview of ACE-Asia: Strategies for quantifying the relationships between Asian aerosols and their climatic impacts. *J. Geophys. Res.* 108(D23): 8633, doi:10.1029/2003JD003550.

Ignatov A and L Stowe (2000) Physical basis, premises, and self-consistency checks of aerosol retrievals from TRMM VIRS. *J. Appl. Meteor.* 39(12): 2259–2277.

Ignatov A, L Stowe, SM Sakerin, and GK Korotaev (1995a) Validation of the NOAA/NESDIS satellite aerosol product over the North Atlantic in 1989. *J. Geophys. Res*. 100(D3): 5123–5132.

Ignatov A, L Stowe, R Singh, D Kabanov, and I Dergileva (1995b) Validation of NOAA AVHRR aerosol retrievals using sun-photometer measurements from RV Akademik Vernadsky in 1991. *Adv. Space Res*. 16(10): 95–98.

International Global Atmospheric Chemistry Project (IGAC) (1996) Atmospheric aerosols: A new focus of the International Global Atmospheric Chemistry Project. In: PV Hobbs, and BJ Huebert (eds), *IGAC Core Project Office*, Mass. Inst. Technol., Cambridge.

Intergovernmental Panel on Climate Change (IPCC) (2007) Climate change 2007: The physical science basis. Contribution of working group I to the fourth assessment report of the intergovernmental panel on climate change. In: S Solomon, D Qin, M Manning, Z Chen, M Marquis, KB Averyt, M Tignor, and HL Miller (eds), Cambridge University Press, Cambridge, UK and New York, USA, 996.

Jacobowitz H, L Stowe, G Ohring, A Heidinger, K Knapp, and NR Nalli (2003) The Advanced Very High Resolution Radiometer Pathfinder Atmosphere (PATMOS) climate 25 dataset: A resource for climate research. *Bull. Am. Meteor. Soc*. 84: 785–793.

Jeong MJ, and Z Li (2005) Quality, compatibility, and synergy analyses of global aerosol products derived from the advanced very high resolution radiometer and Total Ozone Mapping Spectrometer. *J. Geophys. Res*. 110, D10S08, doi:10.1029/2004JD004647.

Jeong MJ, Z Li, DA Chu, and SC Tsay (2005). Quality and compatibility analyses of global aerosol products derived from the advanced very high resolution radiometer and Moderate Resolution Imaging Spectroradiometer, *J. Geophys. Res*. 110, D10S09, doi:10.1029/2004JD004648.

Josset D, J Pelon, A Protat, and C Flamant (2008) New approach to determine aerosol optical depth from combined CALIPSO and CloudSat ocean surface echoes. *Geophys. Res. Lett*. 35, L10805, doi:10.1029/2008GL033442.

Kahn RA, BJ Gaitley, JV Martonchik, DJ Diner, KA Crean, and B Holben (2005) Multiangle Imaging Spectroradiometer (MISR) global aerosol optical depth validation based on 2 years of coincident Aerosol Robotic Network (AERONET) observations. *J. Geophys. Res*. 110, D10S04, doi:10.1029/2004JD004706.

Kaufman YJ and RS Fraser (1983) Light extinction by aerosols during summer air pollution, *J. Appl. Meteorol*. 22: 1694–1706.

Kaufman YJ and JH Joseph (1982) Determination of Surface Albedos and Aerosol Extinction Characteristics from Satellite Imagery. *J. Geophys. Res.* 87(C2): 1287–1299.

Kaufman YJ, D Tanré, and O Boucher (2002) A satellite view of aerosols in the climate system. *Nature*. 419: 215–223.

Kaufman YJ, D Tanré, LA Remer, EF Vermote, A Chu, and BN Holben (1997) Operational remote sensing of tropospheric aerosol over land from EOS moderate resolution imaging spectroradiometer. *J. Geophys. Res.* 102(D14): 17051–17067.

Kent GS, CR Trepte, KM Skeens, and DM Winker (1998) LITE and SAGE II measurements of aerosols in the southern hemisphere upper troposphere. *J. Geophys. Res.* 103(D15): 19111–19127.

Kim J, J Lee, HC Lee, A Higurashi, T Takemura, and CH Song (2007) Consistency of the aerosol type classification from satellite remote sensing during the Atmospheric Brown Cloud–East Asia Regional Experiment campaign. *J. Geophys. Res.* 112, D22S33, doi:10.1029/2006JD008201.

King MD, YJ Kaufman, D Tanré, and T Nakajima (1999) Remote sensing of tropospheric aerosols from space: Past, present, and future. *Bull. Am. Meteorol. Soc.* 80: 2229–2259.

Knapp KR, R Froulin, S Kondragunta, and AI Prados (2005) Towards aerosol optical depth retrievals over land from GOES visible radiances: Determining surface reflectance. *Int. J. Remote Sens*. 26(18): 4097–4116.

Knapp KR and LL Stowe (2002) Evaluating the potential for retrieving aerosol optical depth over land from AVHRR pathfinder atmosphere data. *J. Atmos. Sci.* 59(3): 279–293.

Knapp KR, TH Vonder Harr, and YJ Kaufman (2002) Aerosol optical depth retrieval from GOES-8: Uncertainty study and retrieval validation over South America. *J. Geophys. Res*. 107(D7): 4055, doi:10.1029/2001JD000505.

Knapp, KR (2002) Quantification of aerosol signal in GOES 8 visible imagery over the United States. *J. Geophys. Res.* 107(D20): 4426, doi:10.1029/2001JD002001.

Kokhanovsky AA, FM Breon, A Cacciari, E Carboni, D Diner, WD Nicolantonio, RG Grainger, WMF Grey, R Höller, KH Lee, Z Li, PRJ North, A Sayer, G Thomas, W von Hoyningen-Huene (2007) Aerosol remote sensing over land: Satellite retrievals using different algorithms and instruments. *Atmos. Res.* 85: 372–394.

Kokhanovsky AA and G de Leeuw (2009) Satellite aerosol remote sensing over land, Berlin, Springer-Praxis.

Lazarev AI, VV Kovalenok, and SV Avakyan (1987) Investigation of Earth from manned spacecraft, Leningrad, Gidrometeoizdat.

Lee KH, YJ Kim, and W. von Hoyningen-Huene (2004) Estimation of regional aerosol optical thickness from satellite observations during the 2001 ACE-Asia IOP. *J. Geophys. Res.* 109 D19S16, doi:10.1029/2003JD004126

Lee KH, JE Kim, YJ Kim, J Kim, and W von Hoyningen-Huene (2005) Impact of the smoke aerosol from Russian forest fires on the atmospheric environment over

Korea during may 2003. *Atmos. Environ.* 39(2): 85–99, doi:10.1016/j.atmosenv.2004.09.032.

Lee KH, YJ Kim, and MJ Kim (2006a) Characteristics of aerosol observed during two severe haze events over Korea in June and October 2004. *Atmos. Environ.* 40: 5146–5155. doi:10.1016/j.atmosenv.2006.03.050.

Lee KH, YJ Kim, W von Hoyningen-Huene, and JP Burrows (2006b) Influence of land surface effects on MODIS aerosol retrieval using the BAER method over Korea. *Int. J. Remot. Sens.* 27(14): 2813–2830.

Lee KH, YJ Kim, W von Hoyningen-Huene, and JP Burrows (2007a) Spatio-Temporal Variability of Atmospheric Aerosol from MODIS data over Northeast Asia in 2004. *Atmos. Environ.* 41(19): 3959–3973. doi:10.1016/j.atmosenv.2007.01.048.

Lee DH, KH Lee, and YJ Kim (2006c) Application of MODIS aerosol data for aerosol type classification. *Korean J. Remot Sens.* 22(6): 495–505 (In Korean).

Lee KH, Z Li, MS Wong, J Xin, Y Wang, WM Hao, and F Zhao (2007b) Aerosol single scattering albedo estimated across China from a combination of ground and satellite measurements, *J. Geophys. Res.* 112(D22S15), doi:10.1029/2007JD009077.

Leroy M, JL Deuzé, FM Bréon, O Hautecoeur, M Herman, JC Buriez, D Tanré, S Bouffies, P Chazette, and JL Roujean (1997) Retrieval of atmospheric properties and surface bidirectional reflectances over land from POLDER/ADEOS. *J. Geophys. Res.* 102: 17023–17038.

Levelt P, C Camy-Perret, H Eskes, M van Weele, D Hauglustaine, I Aben, D Tanré, L Lavanant, C Clerbaux, M de Maziere, R Jogma, M Dobber, P Veefkind, J Leon, and P Coheur (2006) A mission for TRopospheric composition and Air Quality (TRAQ), American Geophysical Union, Fall Meeting 2006, abstract #A31B-0888, 2006AGUFM.A31B0888L.

Levy RC, LA Remer, and O Dubovik (2007b) Global aerosol optical properties and application to Moderate Resolution Imaging Spectroradiometer aerosol retrieval over land, *J. Geophys. Res.* 112(D13210), doi:10.1029/2006JD007815.

Levy RC, LA Remer, JV Martins, YJ Kaufman, A Plana-Fattori, J Redemann, PB Russell, and B Wenny (2005) Evaluation of the MODIS aerosol retrievals over ocean and land during CLAMS. *J. Atmos. Sci.* 62: 974–992.

Levy RC, LA Remer, S Mattoo, EF Vermote, and YJ Kaufman (2007a) A second-generation algorithm for retrieving aerosol properties over land from MODIS spectral reflectance. *J. Geophys. Res*. 112(D13211).

Li Z, A Khananian, R Fraser, and J Cihlar (2001) Automatic detection of fire smoke using artificial neural networks and threshold approaches applied to AVHRR imagery. *IEEE Trans. Geosci. Remote Sens.* 39: 1859–1870.

Li Z, F Niu, KH Lee, J Xin, WM Hao, B Nordgren, Y Wang, and P Wang (2007) Validation and understanding of MODIS aerosol products using ground-based measurements from the handheld sunphotometer network in China. *J. Geophy. Res.* 112(D22S07), doi:10.1029/2007JD008479.

Liu Y, JA Sarnat, BA Coull, P Koutrakis, and DJ Jacob (2004) Validation of Multiangle Imaging Spectroradiometer (MISR) aerosol optical thickness measurements using Aerosol Robotic Network (AERONET) observations over the contiguous United States. *J. Geophys. Res.* 109(D06205), doi:10.1029/2003JD003981.

Martonchik JV and DJ Diner (1992) Retrieval of aerosol and land surface optical properties from multi-angle satellite imagery. *IEEE Trans. Geosci. Remote Sens.* 30: 223–230.

Martonchik JV, DJ Diner, KA Crean, and MA Bull (2002) Regional aerosol retrieval results from MISR. *IEEE Trans. Geosci. Remote Sens.* 40: 1520–1531.

Martonchik JV, DJ Diner, RA Kahn, TP Ackerman, MM Verstraete, B Pinty, and HR Gordon (1998) Techniques for the retrieval of aerosol properties over land and ocean using multiangle imaging. *IEEE Trans. Geosci. Remote Sens*. 36: 1212–1227.

Martonchik JV, DJ Diner, R Kahn, B Gaitley, and BN Holben (2004) Comparison of MISR and AERONET aerosol optical depths over desert sites. *Geophys. Res. Lett.* 31(L16102), doi:10.1029/2004GL019807.

McCormick MP, P Hamill, TJ Pepin, WP Chu, TJ Swissler, and LR McMaster (1979) Satellite studies of the stratospheric aerosol. *Bull. Am. Meteorol. Soc*. 60(9):1038–1046.

McCormick MP, DM Winker, EV Browell, JA Coakley, CS Gardner, RM Hoff, GS Kent, SH Melfi, RT Menzies, CMR Menzies, DA Randall, and JA Reagan (1993) Scientific investigations planned for the Lidar In-space Technology Experiment (LITE). *Bull. Am. Meteorol. Soc.* 74(2): 205–214.

McPeters, RD, PK Bhartia, AJ Krueger, JR Herman, and O Torres (1996) Nimbus 7 Total Ozone Mapping Spectrometer (TOMS) Data Products User's Guide, NASA Reference Publication.

Mekler Y, H Quenzel, G Ohring, and I Marcus (1977) Relative atmospheric aerosol content from ERTS observations. *J. Geophys. Res*. 82: 967–972.

Mi W, Z Li, X Xia, B Holben, R Levy, F Zhao, H Chen, and M Cribb (2007) Evaluation of the Moderate Resolution Imaging Spectroradiometer aerosol products at two Aerosol Robotic Network stations in China. *J. Geophys. Res*. 112(D22S08), doi:10.1029/2007JD008474.

Mishchenko MI, B Cairns, G Kopp, CF Schueler, BA Fafaul, JE Hansen, RJ Hooker, T Itchkawich, HB Maring, and LD Travis (2007c). Precise and accurate monitoring of terrestrial aerosols and total solar irradiance: Introducing the Glory mission. *Bull. Am. Meteorol. Soc.* 88: 677–691, doi:10.1175/BAMS-88-5-677.

Mishchenko MI, IV Geogdzhayev, B Cairns, WB Rossow, and AA Lacis (1999) Aerosol retrievals over the ocean by use of channels1 and 2 AVHRR data: Sensitivity analysis and Preliminary results. *Appl. Opt*. 38: 7325–7341.

Mishchenko MI, IV Geogdzhayev, WB Rossow, B Cairns, BE Carlson, AA Lacis, L Liu, and LD Travis (2007a) Long-term satellite record reveals likely recent aerosol trend. *Science.* 315(1543), doi:10.1126/science.1136709.

Mishchenko MI and IV Geogdzhayev (2007b) Satellite remote sensing reveals regional tropospheric aerosol trends. *Opt. Express.* 15: 7423–7438.

Moulin C, F Guillard, F. Dulac, and CE Lambert (1997) Long-term daily monitoring of Saharan dust load over marine areas using Meteosat ISCCP-B2 data, Part I: Methodology and preliminary results for the Western Mediterranean. *J. Geophys. Res.* 102: 16947–16958.

Murakami H, K Sasaoka, K Hosoda, H Fukushima, M Toarani, R Frouin, BG Mitchell, M Kahru, PY Deschamps, D Clark, S Flora, M Kishino, S Saitoh, I Asanuma, A Tanaka, H Sasaki, K Yokouchi, Y Kiyomoto, H Saito, C Dupouy, A Siripong, S Matsumura, and J Ishizaka (2006) Validation of ADEOS-II GLI ocean color products using in-situ observations. *J. Oceanogr.* 62: 373–393.

Myhre G, F Stordal, M Johnsrud, DJ Diner, IV Geogdzhayev, JM Haywood, BN Holben, T Holzer-Popp, A Ignatov, R Kahn, YJ Kaufman, N Loeb, J Martonchik, MI Mishchenko, NR Nalli, LA Remer, M Schroedter-Homscheidt, D Tanré, O Torres, M Wang (2005) Intercomparison of satellite retrieved aerosol optical depth over ocean during the period September 1997 to December 2000, *Atmos. Chem. Phys.* 5: 1697–1719.

Myhre G, F Stordal, M Johnsrud, A Ignatov, MI Mishchenko, IV Geogdzhayev, D Tanré, JL Deuzé, P Goloub, T Nakajima, A Higurashi, O Torres, and BN Holben (2004) Intercomparison of satellite retrieved aerosol optical depth over ocean. *J. Atmos. Sci*. 61: 499–513.

Nicolantonio WD, A Cacciari, S Scarpanti, G Ballista, E Morisi, and R Guzzi (2006) SCIAMACHY TOA reflectance correction effects on aerosol optical depth retrieval, Proc. of the First 'Atmospheric Science Conference', ESRIN, Frascati, Italy 8–12 May 2006 (ESA SP-628, July 2006)

Okada Y, S Mukai, and I Sano (2001) Neural network approach for aerosol retrieval. *IGARSS*. 4: 1716–1718.

Palm S, W Hart, D Hlavka, EJ Welton, A Mahesh, and J Spinhirne (2002) GLAS atmospheric data products. GLAS algorithm theoretical basis document (ATBD). Version 4.2. Lanham, MD: Science Systems and Applications, Inc.

Pepin TJ and MP McCormick (1976) Stratospheric Aerosol Measurement – Experiment MA-007, Apollo-Soyuz Test Project, Preliminary Science Report, NASA-JSC, TM-X-58173: 9.1–9.8.

Popp C, A Hauser, N Foppa, and S Wunderle (2007) Remote sensing of aerosol optical depth over central Europe from MSG-SEVIRI data and accuracy assessment with ground-based AERONET measurements. *J. Geophys. Res*. 112(D24S11), doi:10.1029/2007JD008423.

Powell KA, CR Trepte, and GS Kent (1997) Observation of Saharan dust by LITE. In: A Ansmann, R Neuber, P Rairoux, and U Wandinger (eds). *Advances in Atmospheric Remote Sensing with Lidar*, Springer-Verlag, Berlin, 149–152.

Raes F, T Bates, F McGovern, and M VanLiedekerke (2000) The 2nd Aerosol Characterization Experiment (ACE-2): General overview and main results. *Tellus*. 52:111–125.

Randall CE, DW Rusch, JJ Olivero, RM Bevilacqua, LR Poole, JD Lumpe, MD Fromm, KW Hoppel, JS Hornstein, and EPShettle (1996) An overview of POAM II aerosol measurements at 1.06 m. *Geophys. Res. Lett*. 23: 3195–3198.

Rao CRN, EP McClain, and LL Stowe (1989) Remote sensing of aerosols over the oceans using AVHRR data theory, practice, and applications. *Int. J. Remote Sens*. 10(4–5): 743–749.

Remer LA, YJ Kaufman, D Tanré, S Mattoo, DA Chu, JV Martins, RR Li, C Ichoku, RC Levy, RG Kleidman, TF Eck, E Vermote, BN Holben (2005) The MODIS aerosol algorithm, products and validation, *J. Atmos. Sci.* 62: 947–973.

Remer L, D Tanré, and YJ Kaufman (2006) Algorithm for Remote Sensing of Tropospheric Aerosols from MODIS: Collection 5, Algorithm Theoretical Basis Document, http://modis.gsfc.nasa. 5 gov/data/atbd/atmos atbd.php.

Rossow WB, AW Walker, DE Beuschel, and MD Roiter (1996) International Satellite Cloud Climatology Project ~ISCCP documentation of new cloud data sets, World Climate Research Programme Rep. WMOyTD 737 ~World Meteorological Organization, Geneva, Switzerland.

Russell III JM, LL Gordley, JH Park, SR Drayson, WD Hesketh, RJ Cicerone, AF Tuck, JE Frederick, JE Harries, and PJ Crutzen (1993) The halogen occulation experiment. *J. Geophys. Res.* 98(D6): 10,777–10,797.

Russell PB, PV Hobbs, and LL Stowe (1999) Aerosol properties and radiative effects in the United States East Coast haze plume: An overview of the Tropospheric Aerosol Radiative Forcing Observational Experiment (TARFOX). *J. Geophys. Res.* 104(D2): 2213–2222.

Smith RC and KS Baker (1981) Optical properties of the clearest natural waters. *Appl. Opt*. 20: 177–184.

Spinhirne JD, SP Palm, WD Hart, DL Hlavka, and EJ Welton (2005b) Cloud and aerosol measurements from GLAS: Overview and initial results. *Geophys. Res. Lett*. 32(L22S03), doi:10.1029/2005GL023507.

Spinhirne JD, SP Palm, DL Hlavka, WD Hart, EJ Welton (2005a) Global aerosol distribution from the GLAS polar orbiting lidar instrument. *Remote Sensing of Atmospheric Aerosols, 2005. IEEE Workshop on aerosols*. 2–8, DOI: 10.1109/AERSOL.2005.1494140.

Stowe LL (1991) Cloud and aerosol products at NOAA/NESDIS. *Paleogeogr. Paleoclimatol. Paleoecol*. 90: 25–32.

Stowe LL, AM Ignatov, and RR Singh (1997) Development, validation, and potential enhancements to the second-generation operational aerosol product at the National Environmental Satellite, Data, and Information Service of the National Oceanic and Atmospheric Administration. *J. Geophys. Res.* 102: 16923–16934.

Stowe LL, H Jacobowitz, G Ohring, K Knapp, and N Nalli (2002) The Advanced Very High Resolution Pathfinder Atmosphere (PATMOS) climate dataset: Initial analysis and evaluations. *J. Climate.* 15: 1243–1260.

Tang J, Y Xue, T Yuc, and YN Guan (2005) Aerosol optical thickness determination by exploiting the synergy of TERRA and AQUA MODIS. *Remot Sens. Environ.* 94: 327–34.

Tanré D, YJ Kaufman, M Herman, and S Mattoo (1997) Remote sensing of aerosol properties over oceans using the MODIS/EOS spectral radiances. *J. Geophys. Res.* 102(D14): 16971–16988.

Tanré D, LA Remer, YJ Kaufman, S Mattoo, PV Hobbs, JM Livingston, PB Russell, and A Smirnov (1999) Retrieval of aerosol optical thickness and size distribution over ocean from the MODIS airborne simulator during TARFOX. *J. Geophys. Res.* 104(D2): 2261–2278.

Thomason LW, LR Poole, and CE Randall (2007) SAGE III aerosol extinction validation in the Arctic winter: Comparisons with SAGE II and POAM III. *Atmos. Chem. Phys.* 7: 1423–1433.

Torres O, PK Bhartia, JR Herman, Z Ahmad, and J Gleason (1998) Derivation of aerosol properties from satellite measurements of backscattered ultraviolet radiation: Theoretical basis. *J. Geophys. Res*. 103: 17099.

Torres O, PK Bhartia, JR Herman, A Sinyuk, and B Holben (2002) A long term record of aerosol optical thickness from TOMS observations and comparison to AERONET measurements. *J. Atm. Sci.* 59:398–413.

Torres O, PK Bhartia, A Sinyuk, EJ Welton, and B Holben (2005) Total Ozone Mapping Spectrometer measurements of aerosol absorption from space: Comparison to SAFARI 2000 ground-based observations. *J. Geophys. Res*. 110(D10S18), doi:10.1029/2004JD004611.

Trijonis J, R Charlson, R Husar, WC Malm, M Pitchford, W White (1991) Visibility: Existing and historical conditions – causes and effects. In: *Acid Deposition: State of Science and Technology*. Report 24. National Acid Precipitation Assessment Program.

Vaughan M, S Young, D Winker, K Powell, A Omar, Z Liu, Y Hu, and C Hostetler (2004) Fully automated analysis of space-based lidar data: An overview of the CALIPSO retrieval algorithms and data products. *Proc. SPIE*. 5575: 16–30.

Veefkind JP, G de Leeuw, PA Durkee, PB Russell, PV Hobbs, and JM Livingston (1999) Aerosol optical depth retrieval using ATSR-2 and AVHRR data during TARFOX. *J. Geophys. Res.* 104(D2): 2253–2260.

Veefkind, JP and G de Leeuw (1998) A new aerosol retrieval algorithm to determine the spectral aerosol optical depth from satellite radiometer measurements. *J. Aerosol Sci.* 29: 1237–1248.

Vidot J, R Santer, and O Aznay (2008) Evaluation of the MERIS aerosol product over land with AERONET. *Atmos. Chem. Phys. Discuss*. 8: 3721–3759

Viollier M, D Tanré, and P Deschamps (1980) An algorithm for remote sensing of water color from space. *Boundary Layer Meteorol*. 18: 247–267.

von Hoyningen-Huene W, M Freitag, and JP Burrows (2003) Retrieval of aerosol optical thickness over land surfaces from top-of-atmospher radiance. *J. Geophys. Res*. 108: 4260, doi:10.1029/2001JD002018.

von Hoyningen-Huene W, AA Kokhanovsky, JP Burrows, V Bruniquel-Pinel, P Regner, F Baret (2006) Simultaneous determination of aerosol and surface chracteristics from MERIS top-of-atmosphere reflectance. *Adv. Space Res*. 37: 2172–2177.

von Hoyningen-Huene W, AA Kokhanovsky, M Wuttke, M Buchwitz, S Noel, K Gerilowski, JP Burrows, B Latter, R Siddans, and BJ Kerridge (2005) Validation of SCIAMACHY top-of-atmosphere reflectance for aerosol remote sensing using MERIS L1 data, *Atmos. Chem. Phys. Discuss.* 6: 673–699.

Wang J, SA Christopher, F Brechtel, J Kim, B Schmid, J Redemann, PB Russell, P Quinn, and BN Holben (2003) Geostationary satellite retrievals of aerosol optical thickness during ACE-Asia. *J. Geophys. Res*. 108(D23): 8657, doi:10.1029/2003JD003580.

Wang M, KD Knobelspiesse, and CR McClain (2005) Study of the Sea-Viewing Wide Field-of-View Sensor (SeaWiFS) aerosol optical property data over ocean in combination with the ocean color products. *J. Geophys. Res.* 110(D10S06), doi:10.1029/2004JD004950.

Winker DM, RH Couch, and MP McCormick (1996) An overview of LITE: NASA's Lidar In-space Technology Experiment. *Proc. IEEE.* 84: 164–180.

Zasetsky AY and JJ Sloan (2005) Monte Carlo approach to identification of the composition of stratospheric aerosols from infrared solar occultation measurements. *Appl. Opt*. 44: 4785–4790.